A Vision-based Distance Estimation System for Flying Copters

by

Zetong Li

Thesis submitted to the University of Ottawa
in partial Fulfillment of the requirements for the
M.Sc. degree in
System Science

School of System Science Graduate Program
Faculty of Engineering
University of Ottawa

Abstract

Currently, as one of the most popular technologies being discussed and experimented, the application of flying copters in different industries is facing an obvious barrier; which is how to avoid obstacles while flying. One of the industries among all is small-sized package delivery business, which is also the master topic of a series of experiments. The most popular designs that have used for the Flying Copter Obstacle Avoidance System such as lidar scanners and infrared rangefinders are significantly accurate. However, with the heavyweight, expensive price and higher power consumption, these systems cannot be put into mass production. To reduce the cost and power consumption of the Obstacle Avoidance System, an innovative vision-based low-cost Obstacle Distance Estimation System for flying copters is demonstrated in this thesis. The Fisheye Lens Camera is used to provide a broader detection range and accurate results.

Compared to other standard vision-based systems, the Fish Lens Camera Distance Estimation System can provide (around 360 degrees) extensive view for obstacle detection. Through the parallax pictures captured by the camera and the trigonometric rules, the system can estimate the distance to the target obstacle with reasonable results.

Acknowledgements

I would like to express my sincere gratitude to my supervisors Prof. Tet Yeap and Prof. Iluju Kiringa for their constant support, guidance and encouragement. I am also thankful for their patience, extensive knowledge and constructive comments on my research. Their expertise was invaluable in the formulating of the research topic and methodology in particular. Without the precious support and feedback of my supervisors, it would not be possible to conduct this research. I am so proud to be one of their students.

Special thanks go to my colleagues, Cong Zhao, Junye Yan, Ci Lin, Patrick Killeen, Yi Liu, Wenjie Chen, Shanghao Li and all my friends who helped me during the study here. Finally, I would like to thank my family, my dad Xianhui Li, my mom Ge Tang, my aunt Wen Tang, my sister Qing Yang and Cong Zhao, for their strong support, love and caring which encourages me to continue to achieve my goal.

Table of Contents

List of Tables

List of Figures

List of Abbreviation

3D	Three Dimension
BFLC	Binocular Distance Estimation System
DE	Distance Estimation
DES	Distance Estimation System
fps	Frame per Second
MFLC	Monocular Distance Estimation System
OA	Obstacle Avoidance
OAT	Obstacle Avoidance Technique
OAS	Obstacle Avoidance System
ORB	Oriented FAST and Rotated BRIEF
SIFT	Scale Invariant Feature Transform
SURF	Speeded Up Robust Features

List of Symbols

$\angle$	Angle Symbol
θ	Degree of Angle
ρ	The Corrected Distance of the Distortion Picture
d	Spacing Between Two Cameras

Chapter 1

Introduction

Flying Copter, also known as drone, is controlled by radio remote control equipment or preprogrammed system [1]. Drones are characterized by their flexibility and mobility. They can be widely used on transportation and detection because of the tiny size and light weight [2].

In recent years, with the development of technology, the number of researchers focusing on experimenting on the drone is growing at a fast pace [3]. The maneuverability of drones enables them to be utilized by military force, government programs, and scientific research. Drones are adopted by military force to be used for surveillance and detection, communication and information, electronic countermeasures, navigation, strategic harassment, ground attack, etc. The main use of drone overseas is reconnaissance, tracking enemy/unknown areas or buildings for force protection [4]. In government programs, the drone can be used for geodetic surveys, urban environmental detection, natural disaster monitoring, and cargo transportation. Actively involved in atmospheric research are, meteorological observation, experimental verification of new technologies, equipment and new aircraft with the field of scientific research.

1.1 Problem Description

People mainly use a control panel to fly the drone. but with higher dependence on automation, manual control is unable to satisfy the requirements of having the drones to accomplish tasks on their own. In order to fulfill the growing needs of delivering small-sized packages or items, it is necessary for the drones to have the ability of automatic flying. With the advancement of technology, automatic pilot will certainly replace manual

control flying in the near future. Automated drones must have the feature of 360 degrees surrounding vision detection so that they will not collide with obstacles (including other drones). A reliable Obstacle Avoidance System (OAS) is of utmost importance.

Infrared rangers, lidar detection, and ultrasonic/sonar sensors are currently used for Obstacle Avoidance Techniques (OAT) [2,5–7]. These methods have their advantages, but the manufacturing cost is still the major issue of mass production of the designs. It is unrealistic to expect all drones to be equipped with pricy hardware like Lidar rangers and Infrared sensors.

1.2 Thesis Statement and Contribution

Based on the designs and researches for OAS of drone, this thesis aims to tackle the manufacturing cost and limited power consumption problem of the system. With the considerations above, the low-cost Fisheye Lens camera Distance Estimation System (DES) is presented. With the application of the innovative design, the contributions of this thesis which could improve the overall cost-performance and power consumption can be summarized in the following points:

- Firstly, according to the feature of standard vision-based distance detection/estimation method [8, 9], the system can use either monocular camera or binocular cameras to estimate the distance to the target.
- Secondly, the regular camera lens is about the same price with the Fisheye camera lens; however the Fisheye Lens Camera has a broader field of view than most modern cameras while estimating distance. With the improvement of the sight range, the use of Fisheye Lens Camera can serve the same purpose with better performance under the same budget.
- Thirdly, it is commonly known in this field that the Fisheye Lens Camera requires fairly low power supply, which means it can provide better performance with low consumption.

To operate the DES, the system will calculate the distance by using the trigonometric rules based on the parallax of pictures captured by the Fisheye Lens Camera once the target obstacle is detected. More details will be discussed in Chapter 3.

Although the Fisheye Lens Camera has its disadvantages, for example, it has a larger distortion effect than most regular cameras, which makes it hard to measure the exact

distance to the target. In this thesis, relatively accurate distance values are used to avoid the collision of the drone. Therefore, the distortion effect of the Fisheye Lens Camera is not so critical.

1.3 Thesis Outline

The outline of this thesis can be divided into five parts.

- **Chapter 1** introduced the motivation and objective of this project. The contributions were also presented in this chapter.
- **Chapter 2** shows the literature review and what has been done due to the field of distance estimation for the drone. It shows the Obstacle Avoidance Method in the vision-based field and other fields which are based on Lidar ranger and an ultrasonic sensor. It also gives the difference between this project and other existing methods.
- **Chapter 3** describes more details about this Distance Estimation Method. It shows the mathematical model with Monocular Fisheye Lens Camera and Binocualr Fisheye Lens Cameras. It also compares the difference between these two designs.
- **Chapter 4** presents the experimental setups for Monocular and Binocular Fisheye Lens Camera Distance Estimation Tests. There are two experiments for each test. With all the final results, more reasonable steady-state errors are presented.
- **Chapter 5** deals with the extension of this design and some supporting configurations. With these improvements, the system can cover the full vision detection surrounding the drone with more accurate results in the future.
- **The last episode** concludes the design of this obstacle Distance Estimation System and experiments have been done. It also gives out the future works and method improvements.

Chapter 2

Background and Related Work

Obstacle distance detection and Obstacle Avoidance (OA) have received increased attention from the research field these years. Extensive work has already been done. The conclusions and suggestions that are provided by these works are relevant to the current project and task. All these methods are being developed to enhance the capabilities of the system and it also simplifies the handling of drone. Thus, drones require less training and skill to operate.

The vision-based system is a relatively cost-effective method, and it is also the most appropriate method used in this article. Works that have already been done on the vision-based system will be introduced in the first part of this chapter. Other than the vision system, with so many researches and projects, lidar rangers and ultrasonic systems are the most practical and exciting methods. The second part will discuss how these methods work besides the vision-based system.

2.1 Vision-based Detection

2.1.1 Binocular Camera Detection Technique

Nowadays, more and more OAS use vision-based Distance Estimation (DE) Techniques to achieve the goal. Stereoscopic detection is the main technique, which employs two spaced cameras to simultaneously capture the target and calculate the distance via trigonometry. The stereoscopic view, for example, has been widely used in the Subaru vehicle Eyesight program [10].

In early 2018, research on highway loss data showed that Subaru's Eyesight technology would reduce the pedestrian-related insurance claims rate by 41%. The essential technology of Eyesight is using a pair of stereo coloured cameras on either side of the vehicle's rear-view mirrors which is the basis of the stereoscopic view method. Eyesight continuously scans the road in front of the car, guaranteeing a safe drive. When the system detects and confirms that the approach speed of the preceding vehicle is dangerous, potentially causing an accident, the system will automatically decelerate the car and, if necessary, stop entirely [11].

Stereoscopic view ranging is also increasingly used in the OA Researches with the aim of calculating the target's distance parallax.

Shibarchi at el. [8] tried to use the stereo image method as a proximity detection for their UAVs. The standard Stereoscopic Method has been presented in this article. The system operates the Distance Estimation Method whenever the feature points of the obstacle have been tracked. By using the known focal length, one can identify essential parameters, such as (but not limited to) angle difference related to the tracked obstacle, the spacing between the two cameras, and the distance to the obstruction. Nonetheless as the author said in the article: "For a high accuracy stereo data acquisition system, the camera configuration must satisfy that both of them must face the same direction.", and that is a noticeable weakness in current stereoscopic view systems. As an ordinary camera lens is usually used for stereoscopic ranging, the vision field of this kind of camera is present only on the front side. As a result, the other angles of the drone will have blind spots.

Due to the limitations of the conventional stereoscopic vision system (using ordinary cameras), Shishir Shah and J. K. Aggarwal [9, 12] began research on stereo vision using Fisheye Lens Cameras. Unlike other cameras, Fisheye Lens Cameras have a broader vision field (usually the angle of view is between 100 and 180 degrees) [13]. As a result, applying a Fisheye Lens Camera to binocular ranging will produce unexpected effects; however, since the Fisheye Lens Camera provides a wide-angle view, distortion occurs at the same time. Usually, the distortion of the Fisheye Lens Camera is divided into two types: barrel distortion and pincushion distortion. Barrel distortion, which distorts the imagine to a sphere shape, is the focus of this article. Immediately below is a comparison between a baseline (i.e. no distortion) and barrel distortion picture. [14]

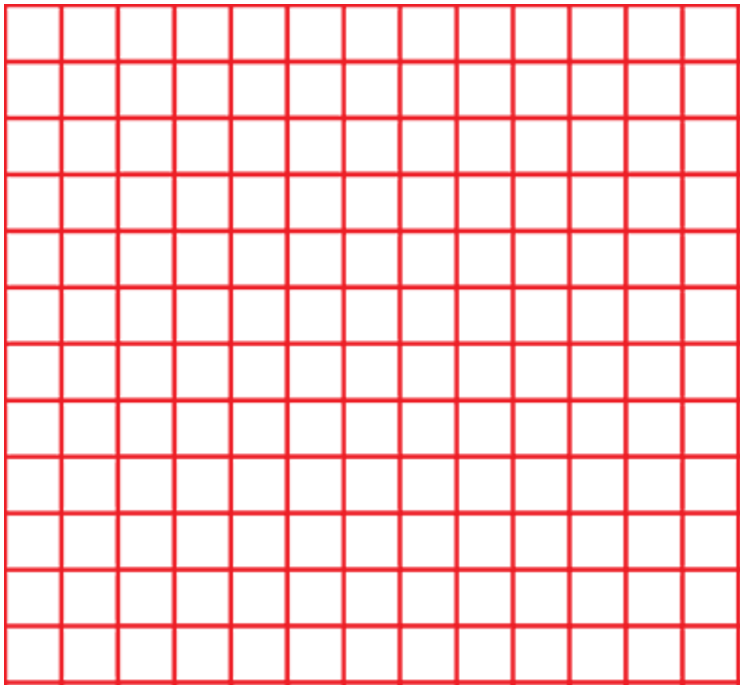

Figure 2.1: Non-distortion picture

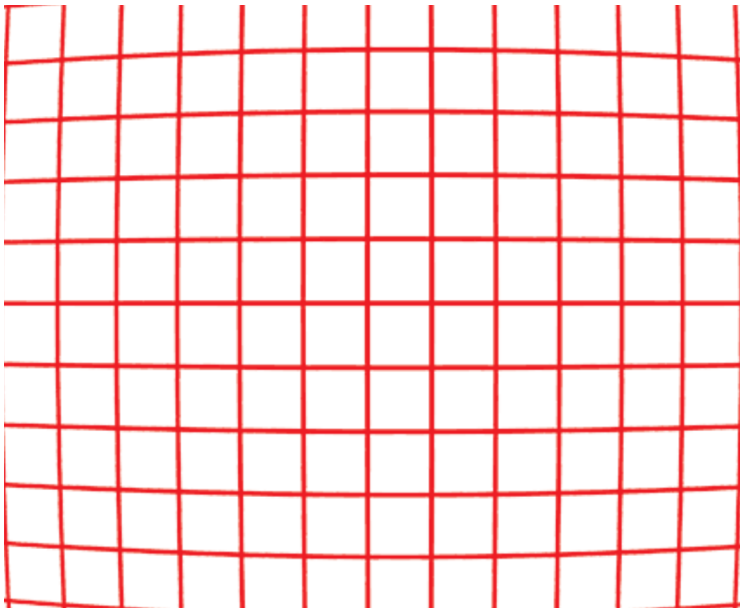

Figure 2.2: Barrel distortion picture

In the paper by Shishir at el., the authors attempt to remove the distortion effect of the Fisheye Lens Camera via algorithms. As the calibration image is made, the distance can be measured by the stereo vision technique. The authors use the following two general equations for the calibration:

$$\theta' = a\theta + b\theta^2 + c\theta^3 + d\theta^4 + e\theta^5[8]$$
$$\rho' = f\rho + g\rho^2 + h\rho^3 + i\rho^4 + j\rho^5[8] \tag{2.1}$$

In the distortion model shown below: "Where θ, the polar angle is defined as the angle subtended by the line joining the projection of any point on the image plane and the optical center in the image plane. θ' is the corrected angle. P is the distance measured from the point projected in the image plane to the optical center while ρ' is the corrected distance." [9] From a to j are the distortion coefficients that will be used in the calibration function.

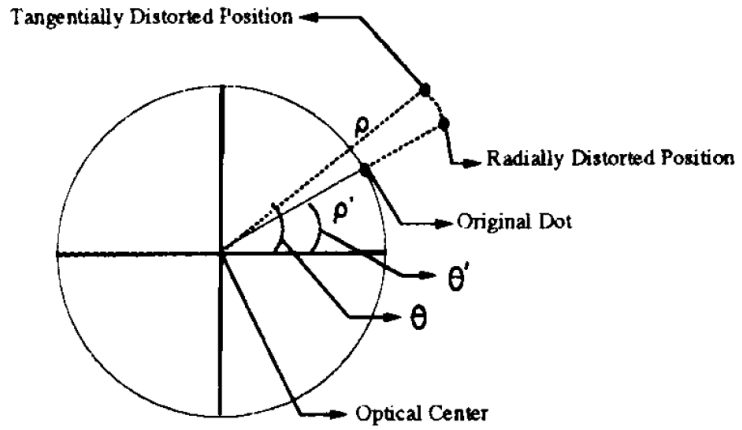

Figure 2.3: The distortion model [8]

Thus, the system not only has a wide-angle view of the Fisheye Lens Camera, but also can measure the precise distance.

With comparing the original image and calibrated image, the corrected image has lapses at the outermost of the barrel distortion. This method; therefore, loses part of the field of view in exchange for more accurate distance monitoring. Consequently, it is not fully capable of 180° obstacle detection.

2.1.2 Monocular Camera Detection Technique

As researching on Stereoscopic View (Binocular Detection) continues to build, researchers have begun trying to use a single camera to attain the OAT of objects. Unlike Stereoscopic View Vision Systems, monocular ranging is cheaper, but the difficulty on distance estimation is correspondingly increased. People start developing methods to match the use

of a single camera. Tomoyuki et al. [15] is one instance of this. The Speeded Up Robust Features (SURF) method has been used to capture the feature points of the picture. By analyzing the feature points distribution of the pixel intensity between images, one can find out if the obstacle is further or closer to their drone effectively increasing collision avoidance.

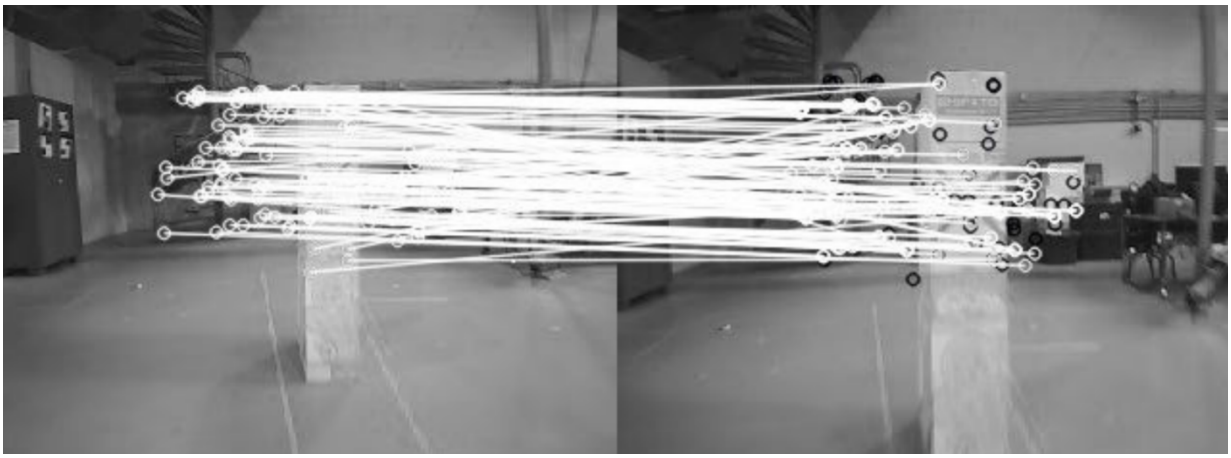

Figure 2.4: The unfiltered SURF matches between the input images [14]

This method has been improved in [16]. In the article, Wilbert G at el. used feature points pixel area detection instead of using pixel distance detection. By computing the relationship between the area and distance $\frac{L_1}{IP_1} = \frac{L_{p1}}{IP_{p1}}$ and $\frac{L_2}{IP_2} = \frac{L_{p2}}{IP_{p2}}$, where L_1 and L_2 are the obstacle lengths, L_{p1} and L_{p2} are the obstacle lengths in pixels. IP_1 and IP_2 are the image plane lengths and the image plane lengths in pixels are represented by IP_{p1} and IP_{p2} [16].

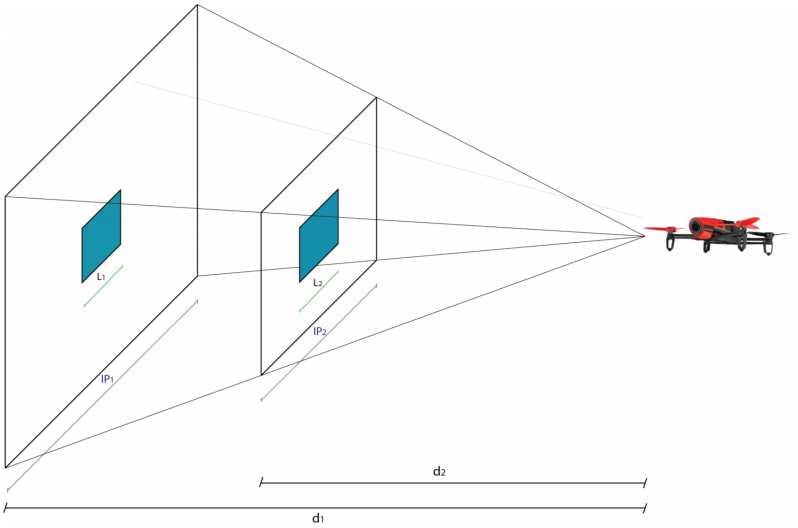

Figure 2.5: Relationship between the area and distance [15]

The monocular camera; however, has only been used in front of the drone. As a result, the OAS is only effective for the field of view directly in front of the drone. Although using a single standard camera for detection lowers the manufacturing costs, it requires a more robust algorithm to control drone flight posture and route planning in case the camera must face the obstacle.

Moreover, if the drone encounters a large object or structure, such as walls, buildings, or the protrusions on the wall, the SURF feature method will struggle to capture valid feature points and match with reference feature points. Where matching is inconsistent, this will undermine the accuracy of the OAS.

To enhance the OAT of the monocular camera, Arjun et al. used the Fisheye Lens Camera in [17]. The camera has the advantages of small size and broad viewing range. In terms of the monocular OAS, it will significantly improve the OAT on the drone, but the barrel distortion is also one of the features of the Fisheye Lens Camera. As a result, it cannot capture the target and detect the distance like a standard camera.

By using OpenCV's distortion calibration method [18], the distorted picture has been fixed. Compared with the photos taken by ordinary cameras, the dewarped images provide more information.

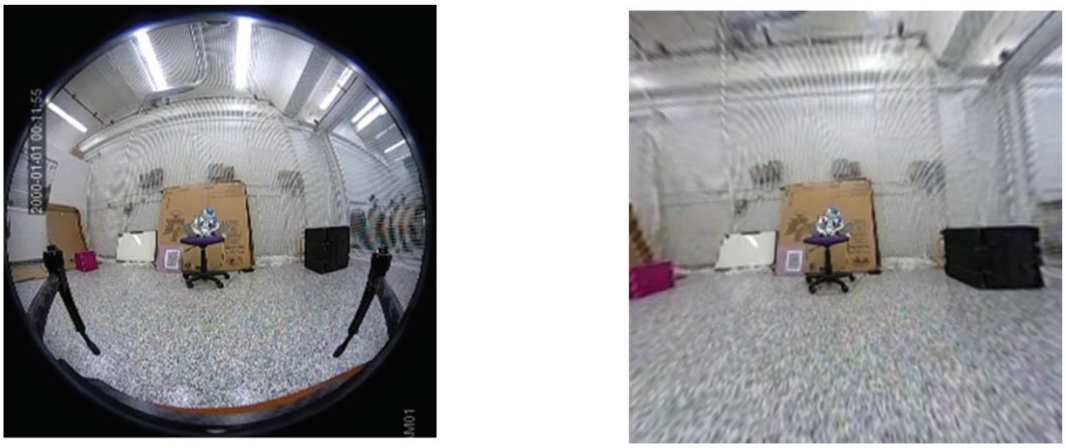

Figure 2.6: **i)** Original image and **ii)** Dewarped image [16]

In this system, the feature points detection algorithm has also been used to detect and extract the target's features. Rather than using the SURF algorithm, with its higher processing speed, the ORB algorithm was instead employed. As feature points of the object are captured, the movement of the object should be distinct, and then the fundamental matrix (F) has been built.

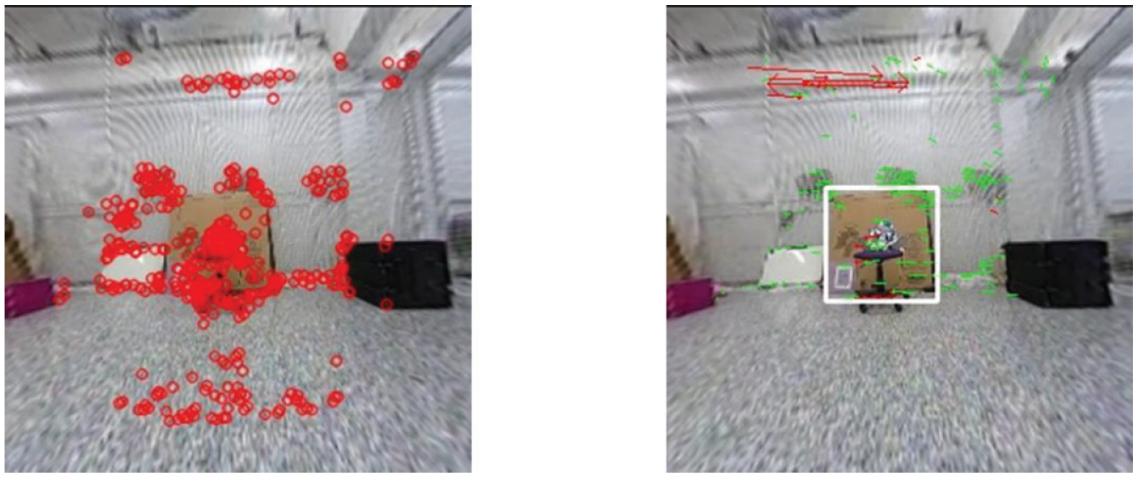

Figure 2.7: **i)** ORB feature points and **ii)** Feature point disparity between two images [16]

The system uses the matrix and the structure reconstruction technique to calculate the position of the image points. Due to the fact that the 3D positions are on an unknown scale, the authors use IMU/GPS data to then convert these image points into realistic scale units. This allows the distance to the target to be estimated.

In terms of hardware facilities, the ESCAM QP130 Fisheye Lens Camera has been used. It is a low-cost camera with 12 volts input power and horizontal 185° vertical 185° filed of view. Moreover, DJI Matrice M100 quadrotor and the BeagleBone Black onboard computer have been applied in this project. After many experiments were done, this OAS achieved near-perfect results with a maximum 10% error.

2.2 Other Techniques

2.2.1 Lidar Scanner (Laser Detector and Ranging)

Numerous methods have been used for detection and ranging, including lidar scanning [6]. The term "Lidar" comes from the mixture of "light" and "radar". Similar to regular Radar, Lidar measures the target's distance by illuminating beams of light. Usually, there are pulses of laser lights; it makes the detection more accurate [19]. Seoungjun et al. [2] used Hokuyo Lidar (UTM-30LX scanning laser rangefinders) for their drone.

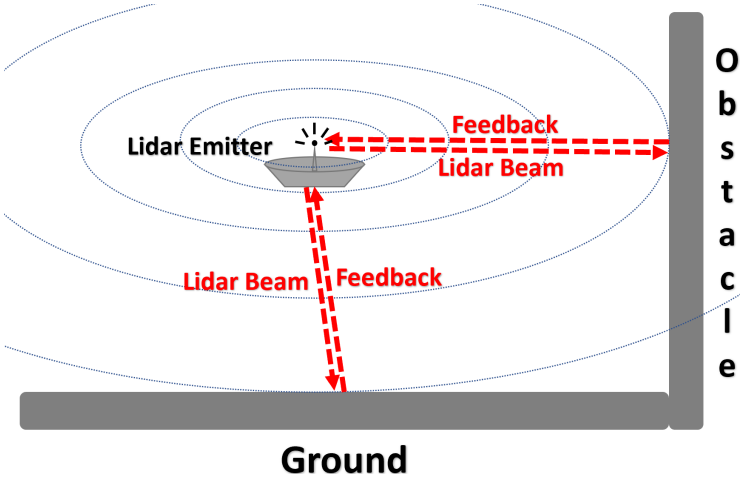

Figure 2.8: Principle of lidar detection

With fast feedback and precise detection, the lidar ranger system is undoubtedly the best detection system compared to other techniques. It can keep scanning the 270 degrees area around itself at a speed of 25 milliseconds per scan [20]. With ±30mm accuracy of distance with the estimation up to 30 meters, the lidar ranger has achieved significant results in long-distance detection.

With the incredibly accurate detection, lidar sensors are more expensive and require greater power consumption to operate the detection system. On the one hand, due to the

high-power consumption, it is not conducive to the sustained endurance of drones. On the other hand, with the high price, if lidar detection will be used on hundreds of drones in the future, that would be a considerable amount of investment.

2.2.2 Ultrasonic Sensor

To lower the manufacturing cost, an ultrasonic sensor has been used. The ultrasonic/sonar sensor can emit soundwaves which has a higher frequency (more than 20kHz). It is a more directional and also a cheaper choice for the drone. Juan et al. [7] used the HC-SR04 ultrasonic sensors to perform a drone OAS that can measure in multiple dimensions. HC-SR04 is an Ultrasonic Range Finder that can provide a 2 cm to 4 meters non-contact measurement with 5 volts low power supply [21]. Due to the low energy consumption, low price, and sound speed feedback features of the HC-SR04 sensor, Juan et al. implemented their drone OAS through it.

Obstacle reflections will be captured if ultrasonic soundwaves encounter some objects on its way. The measured distance can be easily calculated as shown in the figure below.

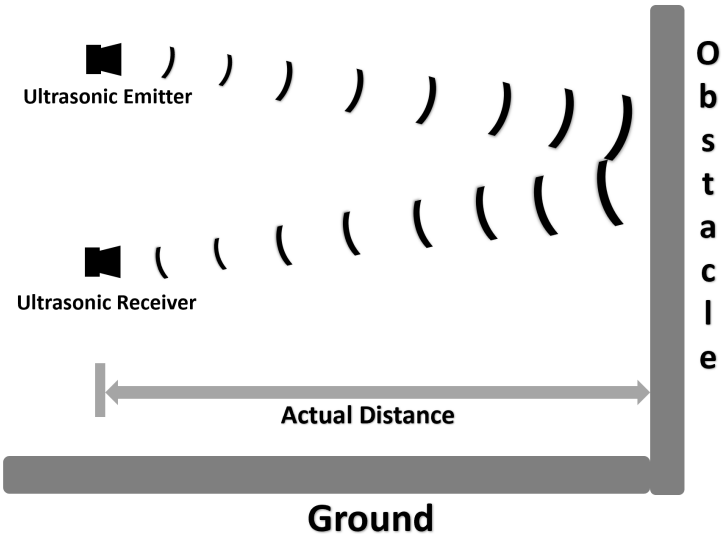

Figure 2.9: Principle of ultrasonic detection

Since the detection range of HC-SR04 can only reach 15 degrees, in order to expand the integrity of the OAS, Juan et al. installed 5 ultrasonic sensors on the drone for multi-angle measurement (in which 4 sensors making horizontal detection on the top of the drone, and one on the bottom to measure the flight height).

Compared to other methods, ultrasonic detection has a lower price point as well as the efficient detection angle and competitive measurement accuracy. Due to the 15 degrees effectual angle, an ultrasonic sensor cannot achieve detections in all directions. Only if multiple sensors are installed. Nils et al. [22] also try to build a low-cost OAS for the drone. In contrast to the avoidance system in Juan et al., they installed both inexpensive ultrasonic and infrared range finders on their drone. As 360 degrees coverage has been made, 16 infrared sensors and 12 ultrasonic sensors were placed on the drone. With numerous sensors now operational, the measurement accuracy significantly improved, but in this case, the increased accuracy was directly correlated with an increase in power consumption and a higher manufacturing cost, both metrics falling above the desired parameters.

Furthermore, the ultrasonic sound waves cannot detect the sound-absorbing surfaces well, such as acoustic wool, clothes, or curtains accurately. It also cannot reliably detect people or the available distance from them. Moreover, ultrasonic sensors will be disturbed by some of the signals or noises and it is easy to get interference from the propellers of the drone.

As a result, the ultrasonic sensors are best employed in indoor drones. However, if the drone performs outdoor detection work, environmental interference will cause a sharp increase in measurement error.

2.3 Introduction of the Drone Distance Estimation System

From conception to realization, every step of the Distance Estimation Function (OA Function) has its place on the drone. Different from vehicles, drones have a more extensive motion range since they can perform 3D flight on the x, y, and z axis.

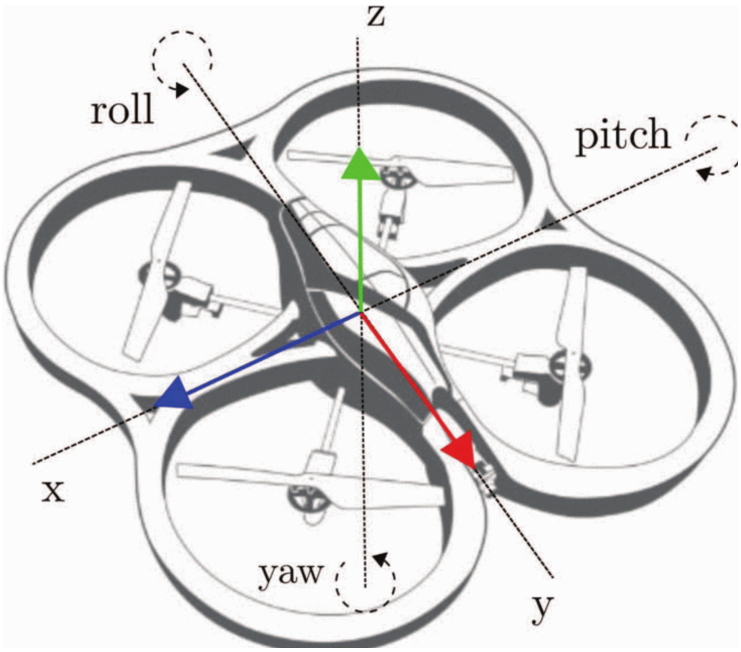

Figure 2.10: 3D flight of the drone

Therefore, the development of drone OAS requires more consideration and higher levels of difficulty. With lower prices and faster feedback, the vision-based system is currently the best-in-class choice for low-cost drone OASs. As mentioned above, most of the research and development relies on standard-camera-based OAS. With the lack of full 720 degrees detection, the drone can easily collide with close by obstacles while avoiding the target ahead. If a machine that can rotate the camera around is installed, it will not only increase the difficulty of research and development for the OAS, but also increase the manufacturing expenses.

Consequently, this project recommends the use of Fisheye Lens Cameras. The Fisheye Lens Camera has a field of view of more than 180 degrees in both the horizontal and vertical axis. If Fisheye Lens Cameras are placed on the top and bottom of the drone, then a 720 degree full-view obstacle detection system is achieved. The goal of this design requires to use the Fisheye Lens Camera to estimate the distance. By using the Fisheye Lens Camera, it can further reduce manufacturing costs while giving the drone a broader field of vision surrounding itself.

Chapter 3

Distance Estimation System for Drone

In this chapter, the detailed theoretical analysis of different designs for the Distance Estimation System (DES) will be presented in the following paragraphs which will be further applied on OAT. Section 3.1 will introduce the assumptions and essentiality of this DES. Section 3.2 introduces the mathematical model of the DES with Binocular Fisheye Lens Cameras (DES-BFLC). Section 3.3 presents the mathematical model of the DES with Monocular Fisheye Lens Camera (DES-MFLC).

3.1 Operation of the System

In order to support the OAT, it is decided that the Fisheye Lens Camera would be a practical and effective hardware for distance detection. Instead of providing rectilinear images, the Fisheye Lens Camera achieves an extremely wide angle of view in comparison to regular cameras. With the ultra wide angle of view, the Fisheye Lens Camera produces strong visual distortion.

To solve the distortion of the image, most of authors who worked with Fisheye Lens Cameras dewarp the distortion image into rectilinear images [9, 17, 18]. But the outermost range of the image is removed while dewarping the distortion pictures.

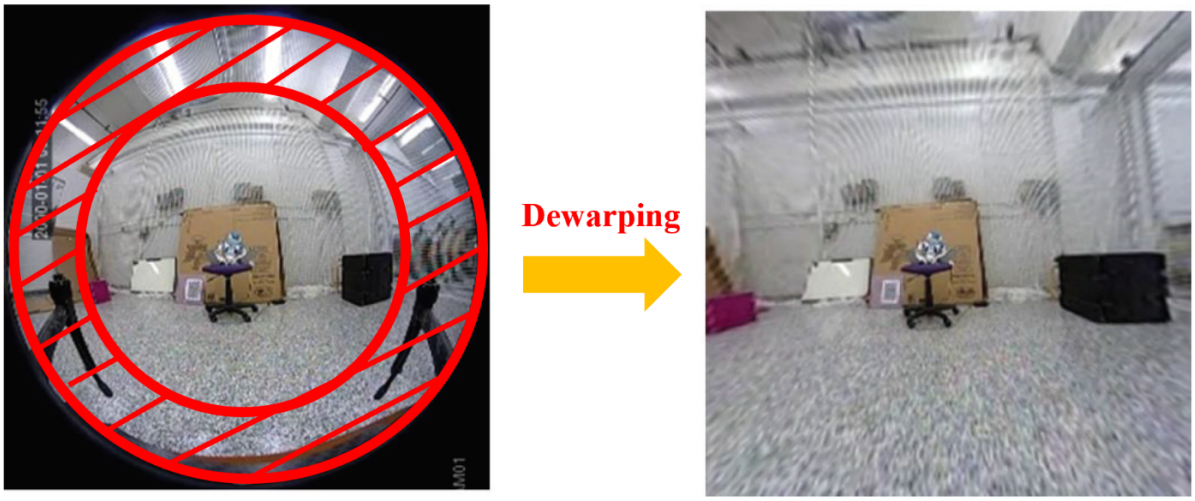

Figure 3.1: Original distortion image (left) and dewarping image (right) (the red circled range in the original image is missing after dewarping the image) [18]

To achieve a wide-angle detection of this DES project, the completeness of the wide-visual images is extremely important; therefore, the Dewarping Technique is not being used in this project.

For the subsections below, the mathematical models of the Fisheye Lens Camera Distance Estimation Technique are described. This technique can be further broken down into DES-BFLC and DES-MFLC. Throughout the technique, the basic assumptions that are used to develop the mathematical model are summarized below:

- The drone can fly in x, y, and z axis
- The drone remains non-stop flying motion
- The system has successfully detected the target obstacle around its flying direction
- The Fisheye Lens Camera installed on the system can capture a picture every 0.1 second (refer to Chapter 4 for more details)
- Flying animals could avoid the drone proactively
- The obstacle is seen as a point for distance estimation

3.2 Binocular Fisheye Lens Camera Detection

To estimate distances to the target obstacle properly, the DES-BFLC Detection Technique has been presented. The figure below shows the structure of the design.

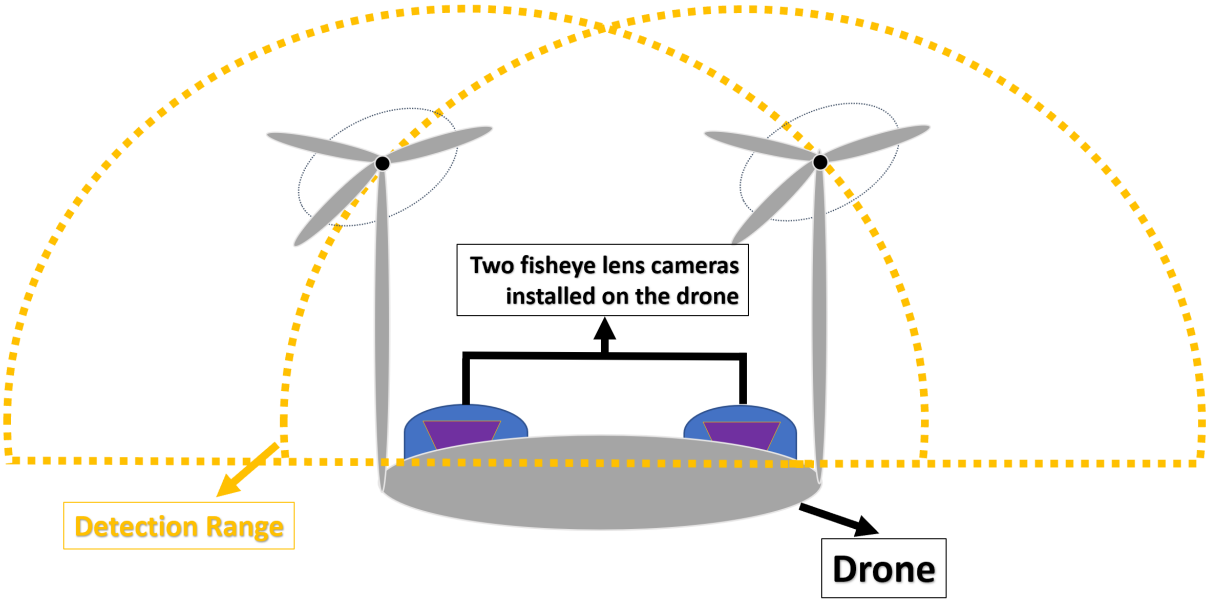

Figure 3.2: DES-BFLC model

As two cameras have been used for detection, the system can measure the distance of the targeted obstacle on a timely basis. Meanwhile, this system can also calculate the speed of the obstacle base on the related distance. The processing procedure of the DES-BFLC is shown in the flowchart below.

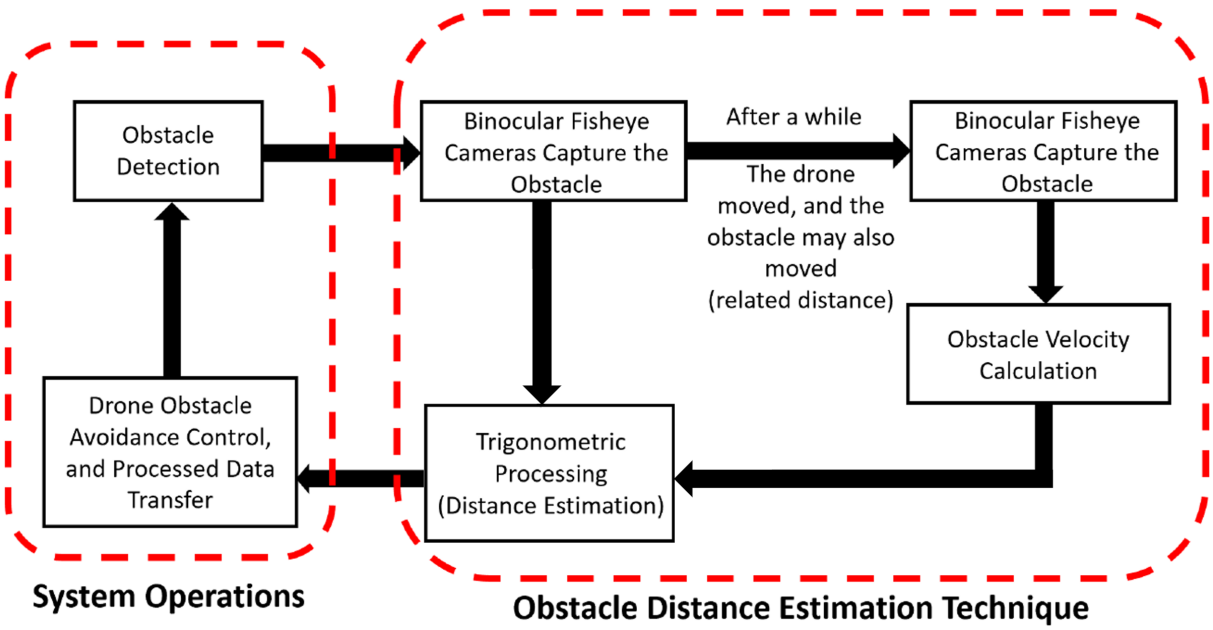

Figure 3.3: Flowchart of DES-BFLC

In this project, it only focuses on the "Obstacle Distance Estimation Technique" part shown above which means an obstacle has already been detected by the cameras before estimating the distance. The "System Operations" part will be completed in the future developments.

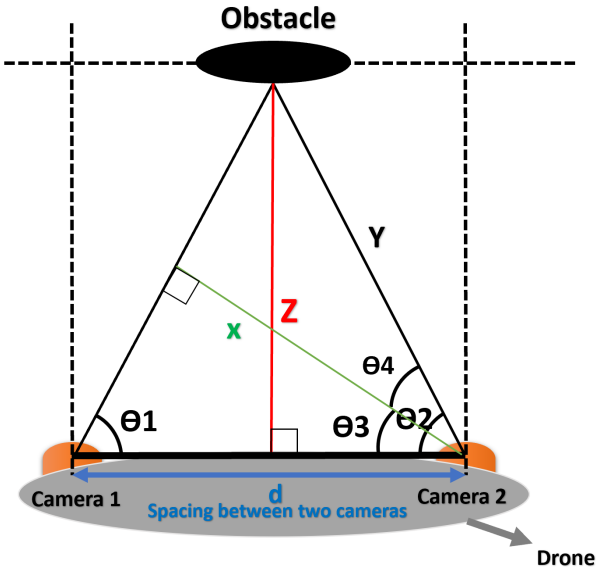

Figure 3.4: Trigonometric model for DES-BFLC

By using two Fisheye Lens Cameras from the stereoscopic view model above, the esti-

mation distance can be calculated instantly. From the Figure, Angle $\theta 1$ and $\theta 2$ represent the angulation between two cameras with the obstacle when cameras simultaneously capture the obstacle. These two angles are known since the obstacle has already been detected. The length d is also a known variable which represents the spacing between two cameras installed on the drone. In this model, Z is the distance result which stands for the distance between the drone and the obstacle. It could be calculated in the following steps:

$$
\begin{aligned}
&Step1 : x = d * \sin\theta 1 \\
&Step2 : \theta 3 = 90^\circ - \theta 1 \\
&Step3 : \theta 4 = \theta 2 - \theta 3 \\
&Step4 : Y = \frac{x}{\cos\theta 4} = \frac{d * \sin\theta 1}{\cos\theta 4} \\
&Step5 : Z = Y * \sin\theta 2 = \frac{d * \sin\theta 1 * \sin\theta 2}{\cos\theta 4}
\end{aligned}
$$

As a result:

$$Z = \frac{d * \sin\theta 1 * \sin\theta 2}{\cos(\theta 2 + \theta 1 - 90^\circ)} \tag{3.1}$$

In this scenario, the estimation result Z can be only applied if the angle of $\theta 1$ and $\theta 2$ both less than 90 degrees. The calculation will be different if any of the two angles are greater than 90 degrees. Situations will be discussed in the following paragraphs:

3.2.1 DES-BFLC - When Angle $\theta 1$ or $\theta 2$ is Greater than 90 Degrees

Since the calculating procedure are similar when angle $\theta 1$ or $\theta 2$ is greater than 90 degrees, only one of the calculations is presented here. The mathematical model when angle $\theta 1$ is greater than 90 degrees has been shown in Figure 3.5 and the calculations has been shown below.

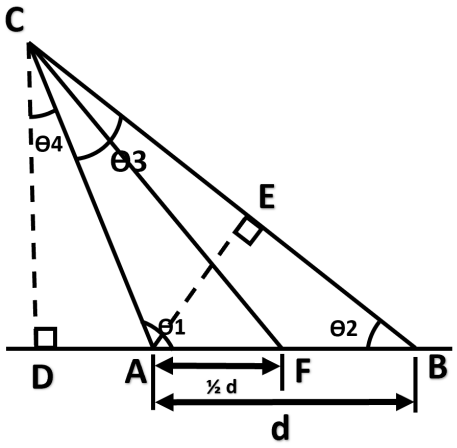

Figure 3.5: Stereoscopic mathematical model when $\theta 1$ is greater than 90 degrees

$$
\begin{aligned}
BE &= \cos\theta 2 * AB \\
AE &= \sin\theta 2 * AB \\
\theta 3 &= 180^\circ - \theta 1 - \theta 2 \\
\tan\theta 3 &= \frac{AE}{CE} \\
CE &= \frac{\sin\theta 2 * AB}{\tan\theta 3} = \frac{\sin\theta 2 * AB}{\tan(180^\circ - \theta 1 - \theta 2)} \\
CB &= CE + BE \\
CB &= \frac{\sin\theta 2 * AB}{\tan(180^\circ - \theta 1 - \theta 2)} + \cos\theta 2 * AB \\
\theta 4 &= 90^\circ - \theta 2 - \theta 3 \\
CD &= \sin\theta 2 * CB \\
DA &= CD * \tan\theta 4 = CB * \sin\theta 2 * \tan\theta 4 \\
CF &= \sqrt{CD^2 + DF^2} = \sqrt{CD^2 + (DA + AF)^2} \\
CF &= \sqrt{(\sin\theta 2 * CB)^2 + (CB * \sin\theta 2 * \tan\theta 4 + \frac{1}{2}d)^2}
\end{aligned}
$$

So, we can have:

$$CF = \sqrt{(\sin\theta 2 * CB)^2 + (CB * \sin\theta 2 * \tan(9^\circ - \theta 2 - \theta 3) + \frac{1}{2}d)^2} \tag{3.2}$$

3.2.2 Obstacle Speed Calculation by DES-BFLC

Since the DES-BFLC has the ability to provide real-time DE, the system is capable to calculate the speed of the target obstacle. The mathematical model of the obstacle speed calculation can be further divided into two cases: when the obstacle moves parallel and nonparallel with the drone. These cases will be discussed separately.

3.2.2.1 Case 1: When the obstacle moves parallel with the drone

Case 1 - Scenario 1: The speed of the drone is faster than the speed of the obstacle

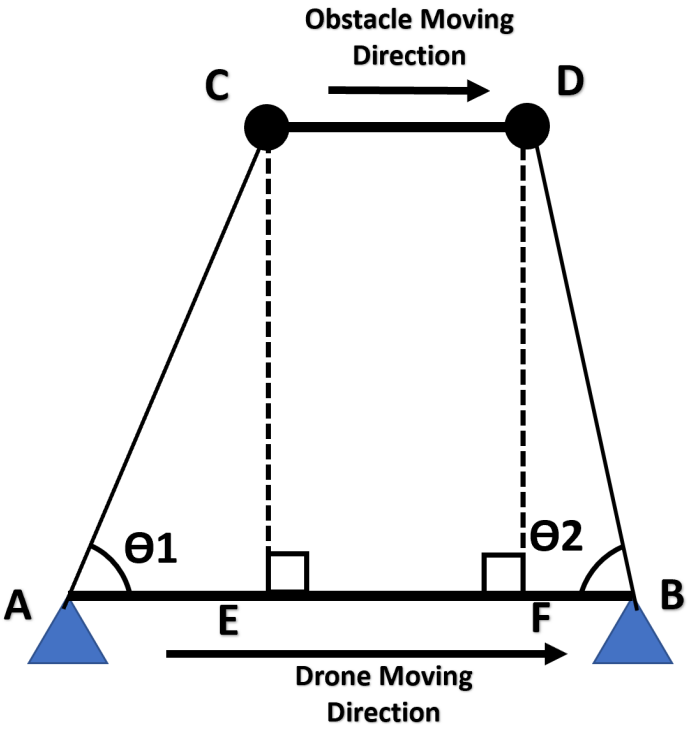

Figure 3.6: Mathematical model when the drone moves faster than the obstacle (parallel)

From Figure 3.6, the blue triangle A represents the drone position when two cameras are capturing the obstacle for the first time. The triangle B represents the position of the drone when the obstacle is being captured after a while. The black circle C and D represents the positions of the obstacle when it is being captured. AC and BD stands for the distance results between the drone and obstacle before and after a time interval. In this case, AC, BD, $\theta 1$, and $\theta 2$ are known variables; therefore, the speed of obstacle can be calculated below.

$$AE = \cos(\theta 1) * AC$$
$$BF = \sin(\theta 2) * BD$$
$$CD = EF = AB - AE - BF$$
$$CD = AB - AC * \cos(\theta 1) - BD * \cos(\theta 2)$$

Speed of the obstacle is:

$$\frac{CD}{0.1second} = \frac{AB - AC * \cos(\theta 1) - BD * \cos(\theta 2)}{0.1second} \tag{3.3}$$

Case 1 - Scenario 2: The speed of the drone is slower than the speed of the obstacle

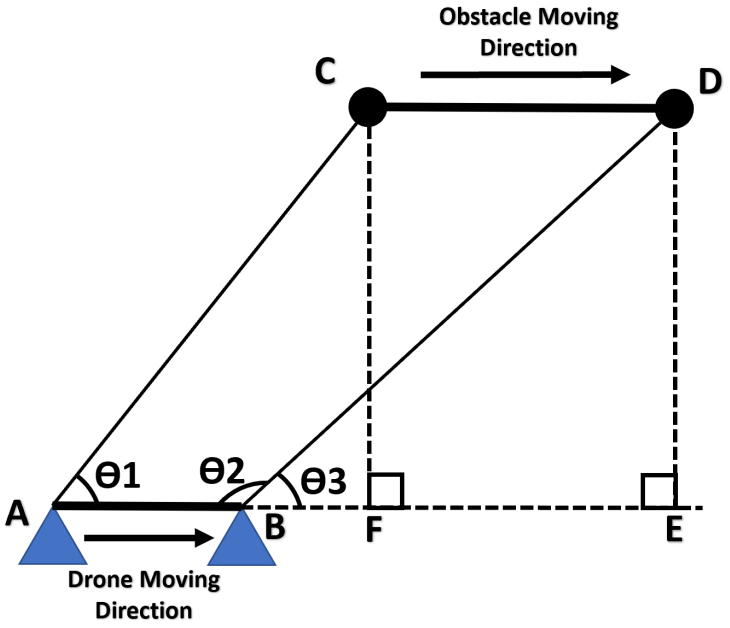

Figure 3.7: Mathematical model when the drone moves slower than the obstacle (parallel)

When the speed of the obstacle is faster, the speed of the obstacle can be calculated in the following steps:

$$\theta 3 = 180^\circ - \theta 2$$
$$BE = \cos(\theta 3) * BD = \cos(180^\circ - \theta 2) * BD$$
$$AE = AB + BE$$
$$AF = \cos(\theta 1) * CA$$
$$CD = EF = AE - AF$$
$$CD = AB + \cos(180^\circ - \theta 2) * BD - \cos(\theta 1) * CA$$

Speed of the obstacle is:

$$\frac{CD}{0.1second} = \frac{AB + \cos(180^\circ - \theta 2) * BD - \cos(\theta 1) * CA}{0.1second} \tag{3.4}$$

3.2.2.2 Case 2: When the obstacle does not moves parallel with the drone

While the drone and the obstacle are moving, the obstacle may not move parallelly with the drone; therefore, this condition has been considered. Same as the section above, it will also discuss the scenarios when the speed of the drone is faster or slower than the speed of the obstacle.

Case 2 - Scenario 1: The speed of the drone is faster than the speed of the obstacle

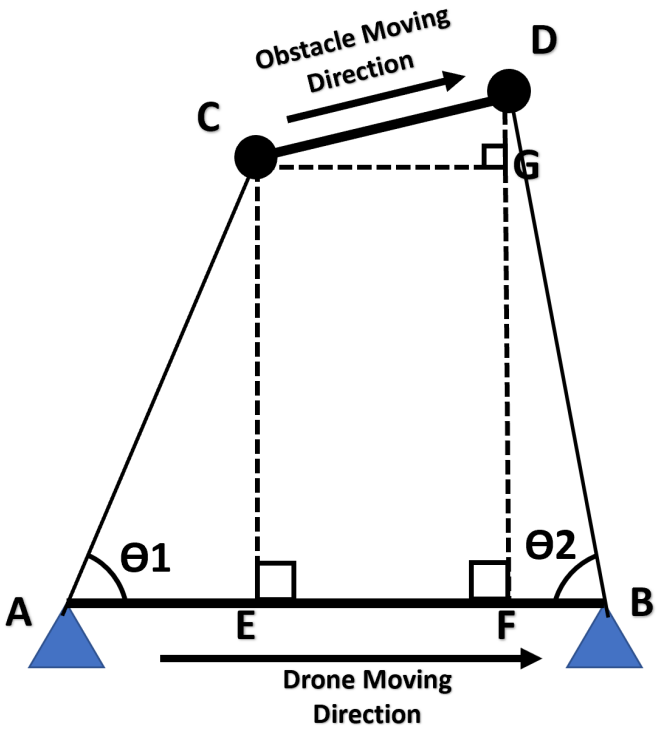

Figure 3.8: Mathematical model when the drone moves faster than the obstacle (nonparallel)

While the speed of the drone is faster, the speed of the obstacle can be calculated in the following steps:

$$CE = \sin(\theta 1) * AC$$
$$DF = \sin(\theta 2) * BD$$
$$DG = EF = DF - CE$$
$$DG = \sin(\theta 2) * BD - \sin(\theta 1) * AC$$
$$AE = \cos(\theta 1) * AC$$
$$BF = \cos(\theta 2) * BD$$
$$CG = EF = AB - AE - BF$$
$$CG = AB - \cos(\theta 1) * AC - \cos(\theta 2) * BD$$
$$CD = \sqrt{CG^2 + DG^2}$$
$$CD = \sqrt{(AB - \cos(\theta 1) * AC - \cos(\theta 2) * BD)^2 + (\sin(\theta 2) * BD - \sin(\theta 1) * AC)^2}$$

Speed of the obstacle is:

$$\frac{CD}{0.1second} =$$

$$\frac{\sqrt{(AB - \cos(\theta 1) * AC - \cos(\theta 2) * BD)^2 + (\sin(\theta 2) * BD - \sin(\theta 1) * AC)^2}}{0.1second} \tag{3.5}$$

Case 2 - Scenario 2: The speed of the drone is slower than the speed of the obstacle

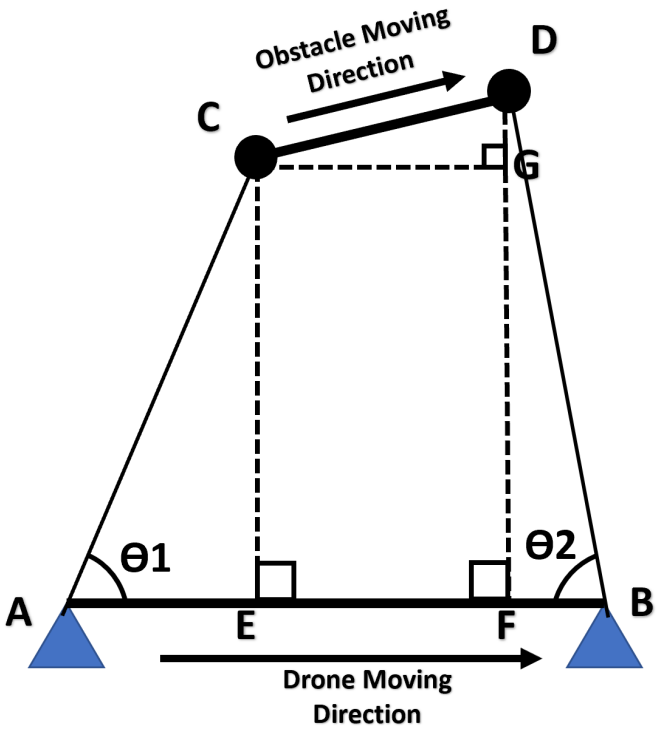

Figure 3.9: Mathematical model when the drone moves slower than the obstacle (nonparallel)

$$\theta 3 = 180^\circ - \theta 2$$
$$DE = \sin(\theta 3) * BD = \sin(180^\circ - \theta 2) * BD$$
$$CF = \sin(\theta 1) * AC$$
$$DG = DE - CF$$
$$DG = \sin(180^\circ - \theta 2) * BD - \sin(\theta 1) * AC$$
$$BE = \cos(180^\circ - \theta 2) * BD$$
$$AE = AB + BE = AB + \cos(180^\circ - \theta 2) * BD$$
$$AF = \cos(\theta 1) * AC$$
$$CG = EF = AE - AF$$
$$CG = AB + \cos(180^\circ - \theta 2) * BD - \cos(\theta 1) * AC$$
$$CD = \sqrt{CG^2 + DG^2}$$
$$CD =$$
$$\sqrt{(AB + \cos(180^\circ - \theta 2) * BD - \cos(\theta 1) * AC)^2 + (\sin(180^\circ - \theta 2) * BD - \sin(\theta 1) * AC)^2}$$

Speed of the obstacle is:

$$\frac{CD}{0.1second} =$$
$$\frac{\sqrt{(AB + \cos(180^\circ - \theta 2) * BD - \cos(\theta 1) * AC)^2}}{0.1second} + \frac{\sqrt{(\sin(180^\circ - \theta 2) * BD - \sin(\theta 1) * AC)^2}}{0.1second} \tag{3.6}$$

3.3 Monocular Fisheye Lens Camera Detection

As the DES-BFLC Detection Technique shown in the section above, two Fisheye Lens Cameras are necessary to be installed on the drone for estimating the distance; however, the DES-BLFC requires a higher hardware purchasing budget and it will use up the battery faster. To further reduce the procurement costs and power consumption, DES-MFLC Detection Technique is introduced in this section. Instead of using two Fisheye Lens Cameras, a single Fisheye Lens Camera is required to complete the DE. The expenditures for purchasing the cameras decrease approximately 50% and with the same battery, the drone will have a longer endurance. The design is shown in the Figure below.

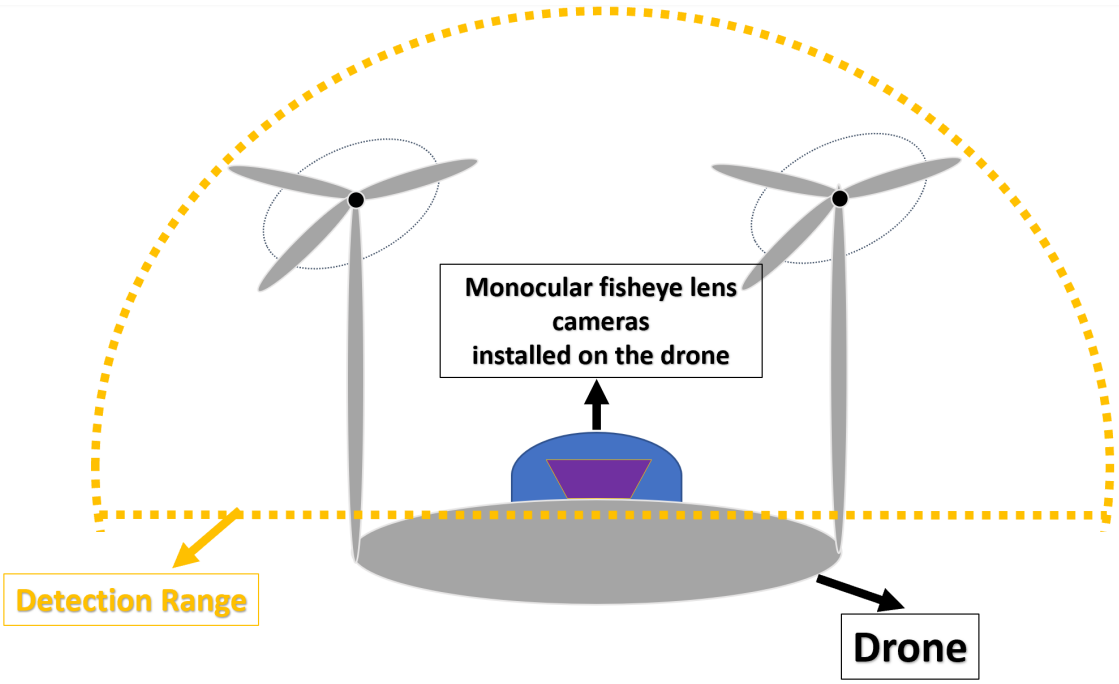

Figure 3.10: DES-MFLC model

The DES-MFLC Detection majorly depends on the drone flying distance and the parallax generated when the system on the flying drone captures the obstacle. According to these characteristics, the DES is achieved through the trigonometric rule.

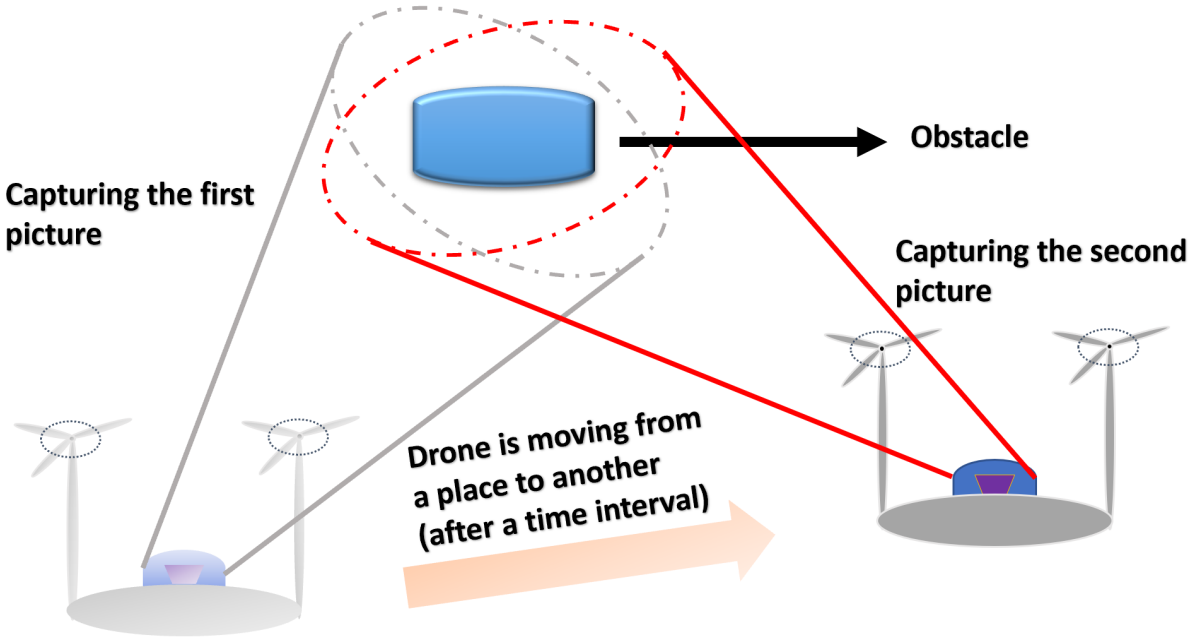

Figure 3.11: DES-MFLC with parallax

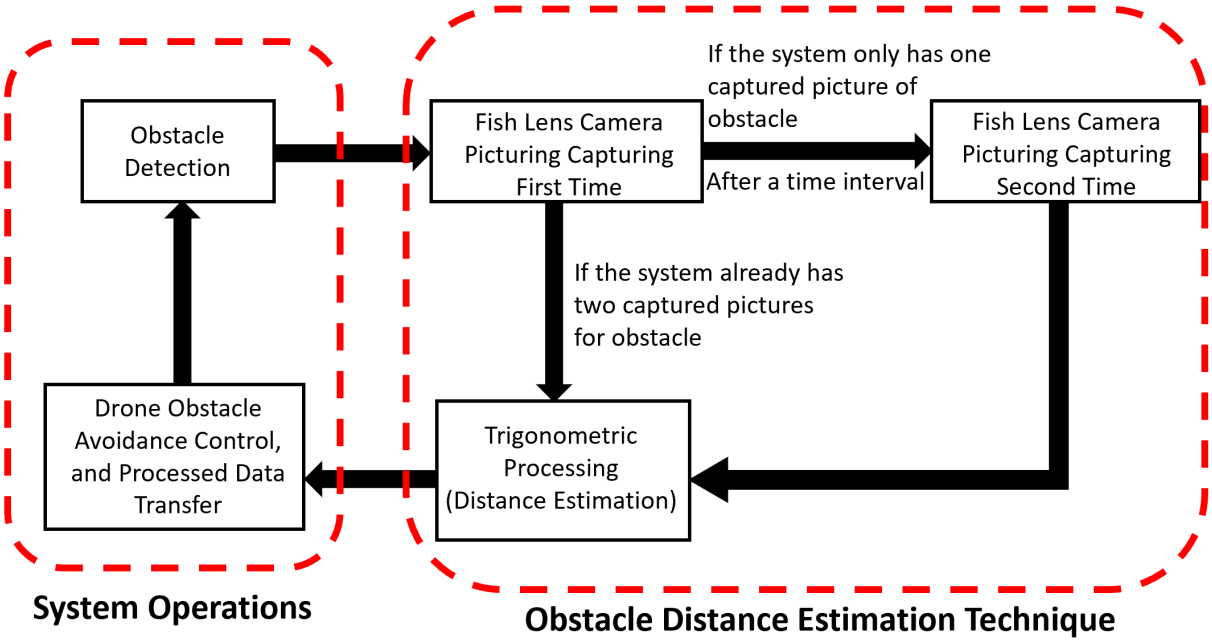

Figure 3.12: Flowchart of DES-MFLC

Additionally, the obstacle may also be stationary or moving while it is captured. Thus, these two cases will be discussed separately in the subsections below.

3.3.1 Case 1: When Target Obstacle is Stationary

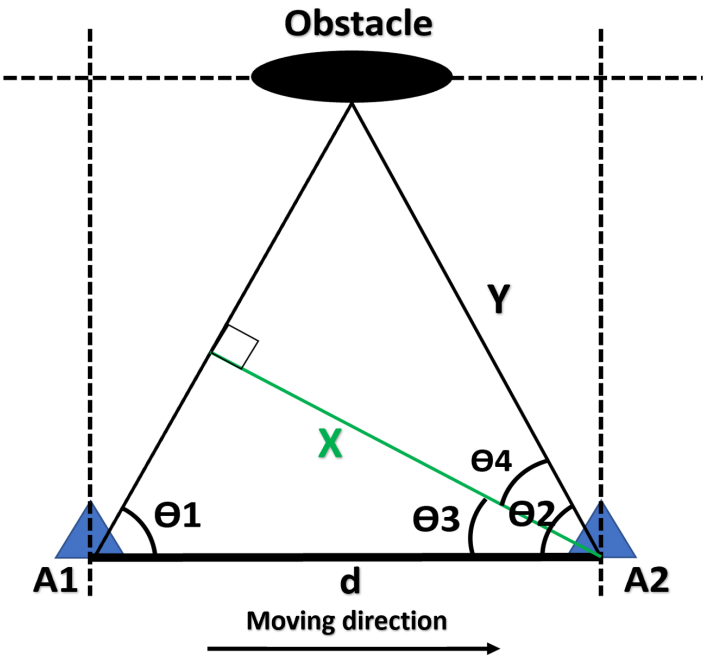

Figure 3.13: Trigonometric model when target obstacle is stationary

In Figure 3.13, the target obstacle is the circle in black and the blue triangles represent the drone which already has been installed in the Fisheye Lens Camera. Triangle $A1$ is the position when the camera first time captures the obstacle drone and triangle $A2$ is the position of the drone after a time interval. $\theta 1$ is the angle when the system detects the obstacle at its position $A1$, and $\theta 2$ is when it detects the obstacle at position $A2$. In this model, $\theta 1$ and $\theta 2$ are known. The distance d can be understood as:

$$d \quad = \quad time \quad interval \quad * \quad speed \quad of \quad drone \tag{3.7}$$

After obtaining these three variables, Y can be calculated by using the trigonometric rule, which is the distance to the obstacle.

$$\begin{aligned} Step \quad & 1 : X = d * \cos\theta 1 \\ Step \quad & 2 : \theta 3 = 90^\circ - \theta 1 \\ Step \quad & 3 : \theta 4 = \theta 2 - \theta 3 \\ Step \quad & 4 : Y = \frac{X}{\cos\theta 4} = \frac{d * \sin\theta 1}{\cos\theta 4} \end{aligned}$$

As a result:

$$Y = \frac{d * \sin\theta 1}{\cos(\theta 2 - \theta 3)} = \frac{d * \sin\theta 1}{\cos(\theta 2 + \theta 1 - 90^\circ)} \tag{3.8}$$

The estimation result y can be only applied to the situation where *angle* $\theta 1$ and $\theta 2$ are both less than 90 degrees. Scenarios when any of the two angles are greater than 90 degrees will be discussed below.

3.3.1.1 Case 1 - Scenario 1: When angle $\theta 1$ is greater than 90 degrees

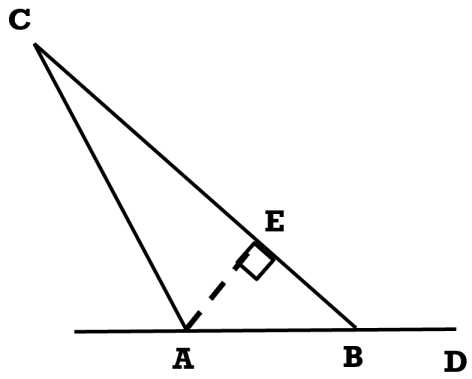

Figure 3.14: Mathematical model when $\theta 1$ ($\angle CAB$) is greater than 90 degrees

In this scenario, angle CAB (equivalent to $\theta 1$ in Figure 3.14), angle CBA (equivalent to $\theta 2$ in Figure 3.14), and line segment AB (equivalent to distance d in Figure 3.14) are known. Then the result of obstacle estimation distance CB can be calculated by the following equations:

$$\begin{aligned}
&BE = \cos(\angle CBA) * AB \\
&AE = \sin(\angle CBA) * AB \\
&\angle ACB = 180^\circ - \angle CAB - \angle CBA \\
&\tan(\angle ACB) = \frac{AE}{CE} \\
&CE = \frac{\sin(\angle CBA) * AB}{\tan(\angle ACB)} = \frac{\sin(\angle CBA) * AB}{\tan(180^\circ - \angle CAB - \angle CBA)} \\
&CB = CE + CB
\end{aligned}$$

As a result:

$$CB = \frac{\sin(\angle CBA) * AB}{\tan(180^\circ - \angle CAB - \angle CBA)} + \cos(\angle CBA) * AB \tag{3.9}$$

3.3.1.2 Case 1 - Scenario 2: When angle $\theta 2$ is greater than 90 degrees

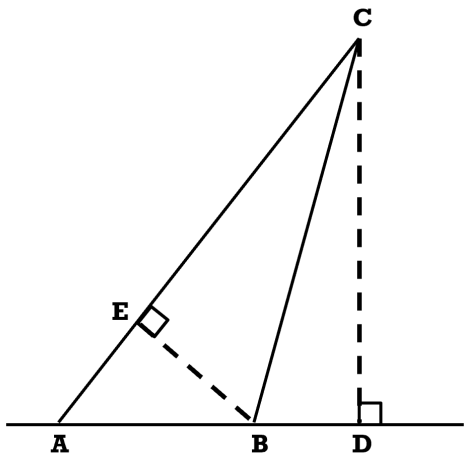

Figure 3.15: Mathematical model when $\theta 2$ ($\angle CBA$) is greater than 90 degrees

Since angle CAB, angle CBA and line segment AB are known, the estimated distance result for CB can be calculated below:

$$\begin{aligned}
BE &= \sin(\angle CBA) * AB \\
\angle CBE &= \angle CBA - \angle EBA \\
\angle CBE &= \angle CBA - (90^\circ - \angle CAB) \\
CB &= \frac{BE}{\cos \angle CBE}
\end{aligned}$$

Consequently,

$$CB = \frac{\sin \angle CAB * AB}{\cos \angle CBA + \angle CAB - 90^\circ} \tag{3.10}$$

3.3.2 Case 2: When Target Obstacle is Moving

In this scenario, the position of the target will change during every photographing interval; therefore, the error of the DES-MFLC Detection increased. To avoid the error expansion, the DES will predict the maximum moving distance of the target for distance estimation

calculation. Since the maximum error produced is only when the target moves in the same direction or the opposite direction to the drone, by assuming the obstacle has the same (maximum) speed as the drone, the DES can calculate two different estimation results (for same and opposite direction). From those two results, the range of the target distance has been defined. The detailed calculation will be described below.

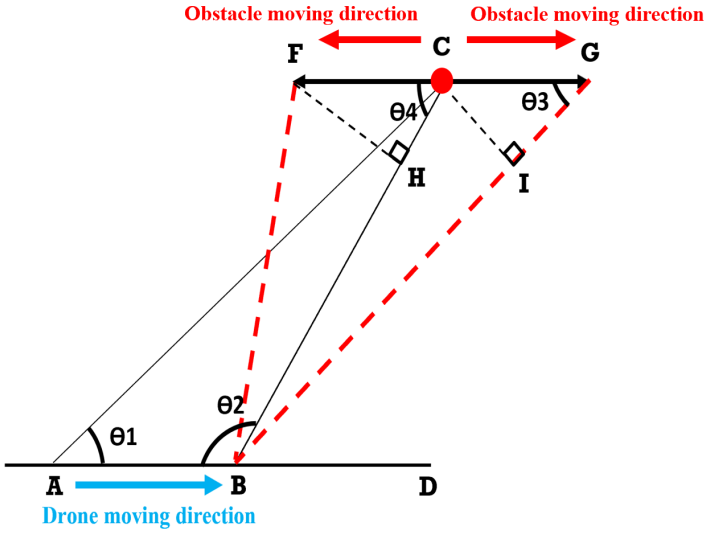

Figure 3.16: Trigonometric model when target obstacle is moving

Figure 3.16 shows the structure of the dynamic target Distance Estimation Method. From the figure, the red point C represents the moving obstacle. The *point* A and *point* B represent the positions of the drone while DES capturing the picture. FC and GC are the moving distance in the opposite direction and the same direction (to the drone). FB and GB represent the two distance results.

Assumption:

- $\theta 1$, $\theta 2$, AB, CB are konwn values
- FG parallel with AB, $\theta 1 = \theta 4$, $\theta 2 = \theta 3$
- $FC = GC = AB$(the obstacle has the same speed of drone)

Calculating FB:

$$
\begin{aligned}
CH &= \cos\theta 4 * FC \\
FH &= \sin\theta 4 * FC \\
HB &= CB - CH = CB - \cos\theta 4 * FC \\
FB &= \sqrt{FH^2 + HB^2}
\end{aligned}
$$

As a result,

$$FB = \sqrt{(\sin\theta 4 * FC)^2 + (CB - \cos\theta 4 * FC)^2} \tag{3.11}$$

Calculating BG:

$$
\begin{aligned}
GI &= \cos\theta 3 * CG \\
CI &= \sin\theta 3 * CG \\
BI &= \sqrt{CB^2 + CI^2} = \sqrt{CB^2 + (\sin\theta 3 * CG)^2} \\
BG &= BI + GI
\end{aligned}
$$

As a result,

$$BG = \sqrt{CB^2 + (\sin\theta 3 * CG)^2} + \cos\theta 3 * CG \tag{3.12}$$

As the distance of FB and BG has been calculated, the distance from the drone to the target will have such range:

$$FB \leqslant TargetDistance \leqslant BG \tag{3.13}$$

Since all the conditions has been discussed above, it can be concluded that the distance drone flies while capturing the obstacle (the length of AB) is the crucial value of the whole Distance Estimation Technique. The length of CB grows with AB gradually. In other words, the longer the distance between the two photos that have been taken, the further the range of the obstacle that can be measured. As AB grows, the obstacle may also move to a further distance which will cost the accuracy of DE. Thus, the value of AB needs to be controlled, since the implementation of real-time feedback and the far-distance detection are indispensable to this project.

Since the DES-MFLC detection cannot give the distance result instantly, it is not able to calculate the speed of the obstacle. Base on the assumption that the camera can take pictures every 0.1 second, the DES-MFLC Detection Method can have an accurate result because the target obstacle cannot make a long-distance movement in such a short time.

Chapter 4

Experimentation and Results

By using the mathematical model in Chapter 3, experimental results are provided in this chapter. More details on experimental setups and steady-state errors are presented in the paragraphs below.

4.1 Experimental Setups

4.1.1 Hardware Setups

For the OAS installed on a drone, the 180 degrees Fisheye Lens Wide Angle Camera [23] is used for distance detection.

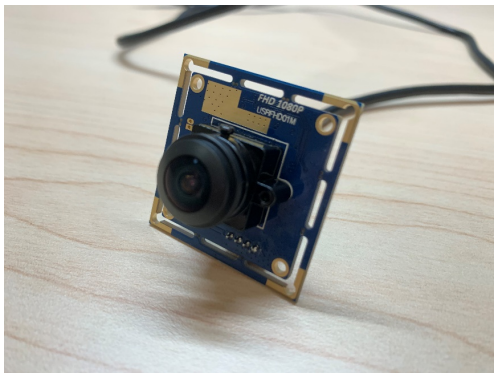

Figure 4.1: 180 degrees Fisheye Lens Wide Angle Camera

Table 4.1: Specifications of the fisheye lens camera [23]

Items Name	180 degrees Fisheye Lens Wide Angle Camera
Size	38 x 38 mm
Field of View	180° Fisheye Super Wide Angel
Frame per Second	Up to 30fps@1080p, 60fps@720P, 100fps@VGA
Frame Resolution	2 megapixel 1920 x 1080p
Item Weight	1.6 Ounces
Power Supply	DC 5V
Item Price	$CAD 45.0

Summarized from Table 4.1, the Fisheye Camera has a smaller size, lower energy consumption, and lightweight. Additionally, compared to other sensors, e.g. the Hokuyo UTM-30LX Lidar sensor (price: $CAD 6181.3) [20], the price of experimented product is much lower and more suitable for mass production.

4.1.2 Essential Data Setup

It is indicated in Table 4.1 that the frame rate of the Fisheye Lens Camera can reach 30 fps (frames per second) in 1080p resolution which means the camera can take 30 photos in one second. As the speed of the drone is about 30 to 40 mph (1341.1 cm/second to 1788.2 cm/second), the OAS can have enough time to process the photo that captured every 0.1 second. In other words, it can provide a spontaneous response and real-time feedback which improves the performance of the system.

With the information above, it can be easily calculated that the drone flies 134.1 cm to 178.8 cm for every 0.1 second; therefore, for getting the most welcomed results, the spacing between the photographs taken by the camera (distance d in Chapter 3) is set in a range of 134.1 cm to 178.8 cm for the experiments below.

4.1.3 Angle Detection Setup

Since the Dewarping Method has not been used for the Fish Lens distortion, the image which is taken by the Fisheye Lens Camera is cylindrically curved. After several experi-

ments, it was noticed that the distortion of images did not cause a significant angle shift. The angles corresponding to each area by the punctuation is shown in the figure below.

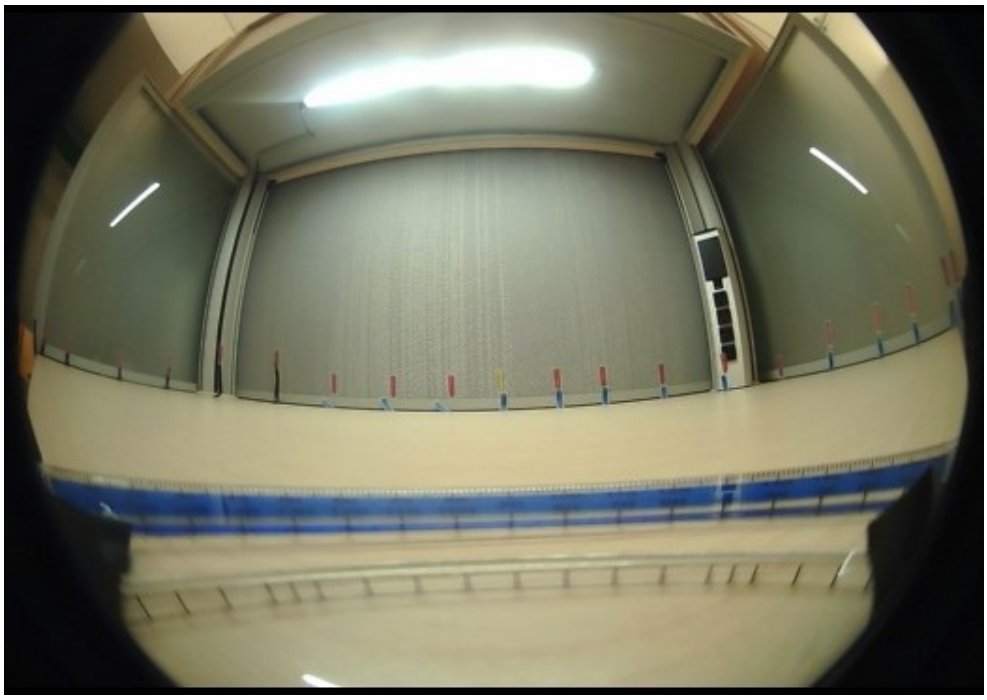

Figure 4.2: Prototype of the scaled snapshot taken by the Fisheye Lens Camera

According to the product parameters of the Fisheye Lens Camera shown in Table 4.1, the maximum horizontal viewing angle of the Fisheye Lens Camera is 180 degrees. The protractor was used for a precise and accurate measurement of this parameter. In Figure 4.2 shown above, every 10 degrees of the protractor was marked on the background, and the camera was placed at the center of the protractor to mimic the detecting position of drones after the future application of the camera.

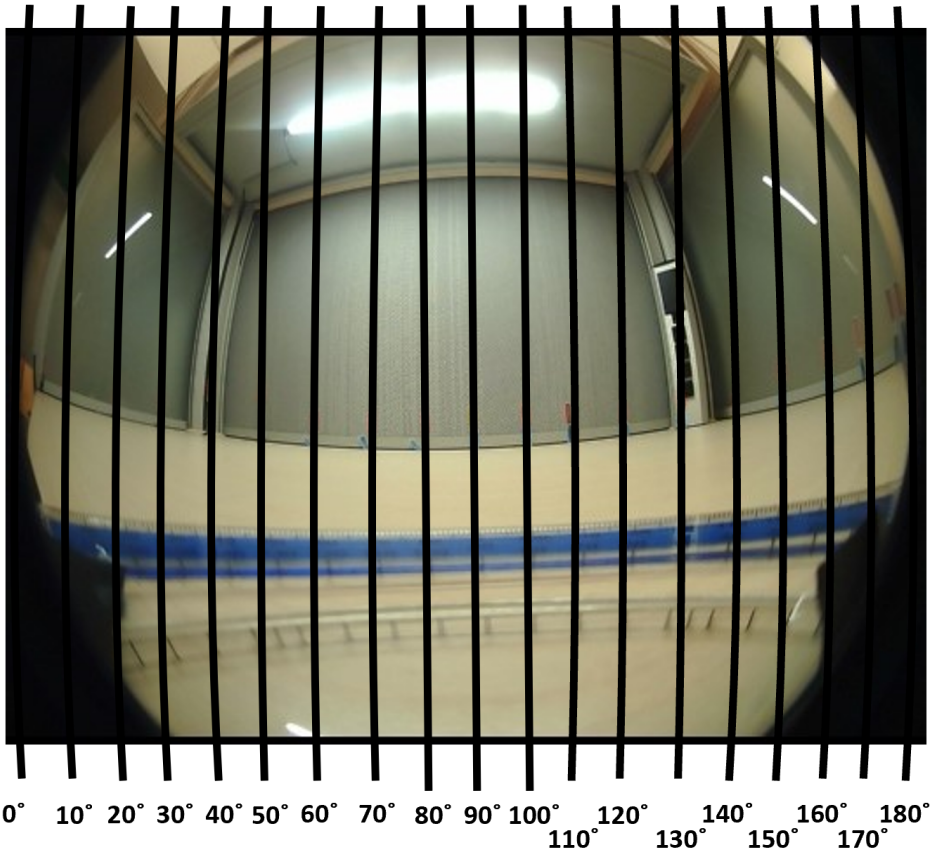

Figure 4.3: The scaled picture taken by the Fisheye Lens Camera (10 degrees as a unit)

Based on the marks shown in Figure 4.3, the error of the angles is around 1 degree per 10 degrees (which included human error). As a result, the 180 degrees horizontal viewing angle of the camera was proved.

By measuring the results repetitively, it can summarize that every 1.2 centimeters correspond to 10 degrees. With this numerical relationship, the angle of the camera (when capturing the picture of the target) can be easily estimated.

4.2 Test Setup and Procedure

The DES experiment was tested under two scenarios: DES-MFLC and DES-BFLC. In the DES-MFLC scenario, the spacing between the photographs will be set between 134.1 centimeters to 178.8 centimeters. A fixed spacing value is used between two cameras for the DES-BFLC scenario.

In the tests below, required angles were marked on it for calculation and distant scaling purposes. (There will only be two experimental results displayed in this section. The rest of the results can be viewed in the [Appendix])

4.2.1 Monocular Fisheye Lens Camera Distance Estimation Test

4.2.1.1 Monocular Distance Estimation – Test 1

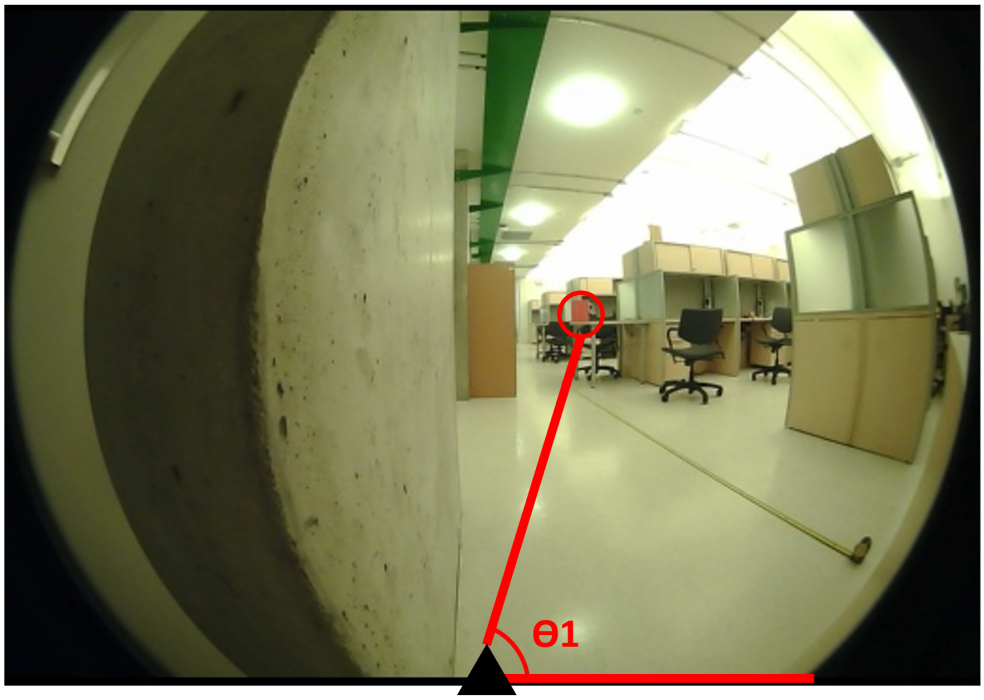

Figure 4.4: Angle $\theta 1$ labeled for DES-MFLC - Test 1

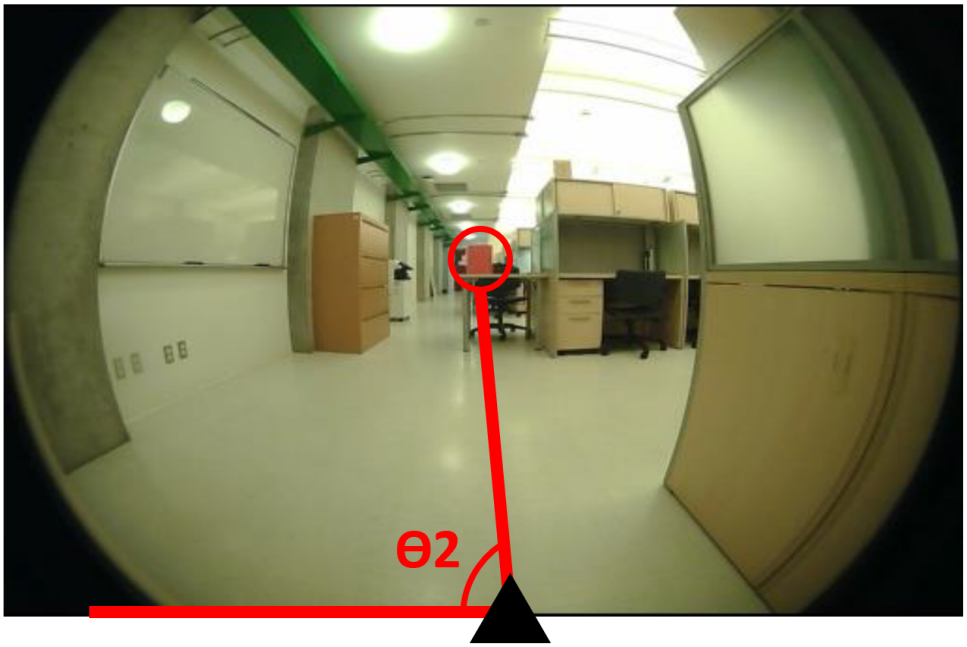

Figure 4.5: Angle $\theta 2$ labeled for DES-MFLC - Test 1

Table 4.2: Experimental results of DES-MFLC - Test 1

Figure #	**Figure 4-4**	**Figure 4-5**
Measured Distance (cm)	426.9 cm	407.9 cm
Spacing between Two Taken Pictures (cm)	165.1 cm	165.1 cm
Degree of Angles (Measured)	78°	83°
Degree of Angles (Experimental)	72.5°	80°
Experimental Distance (cm)		341.1 cm
Percentage Error (%)		16.4%

From the test results above, the marked distance in Figure 4.5 is the measured distance to the target obstacle and the experimental distance for Figure 4.5 is the distance result calculated using equation (3.2) (since both $\theta 1$ and $\theta 2$ are smaller than 90 degrees). In this experiment, with a long-distance-estimation (407.9 centimeters), the error is 16.4%. It showed a favourable result since the target was placed quite far away from the camera.

4.2.2 Monocular Distance Estimation – Test 2

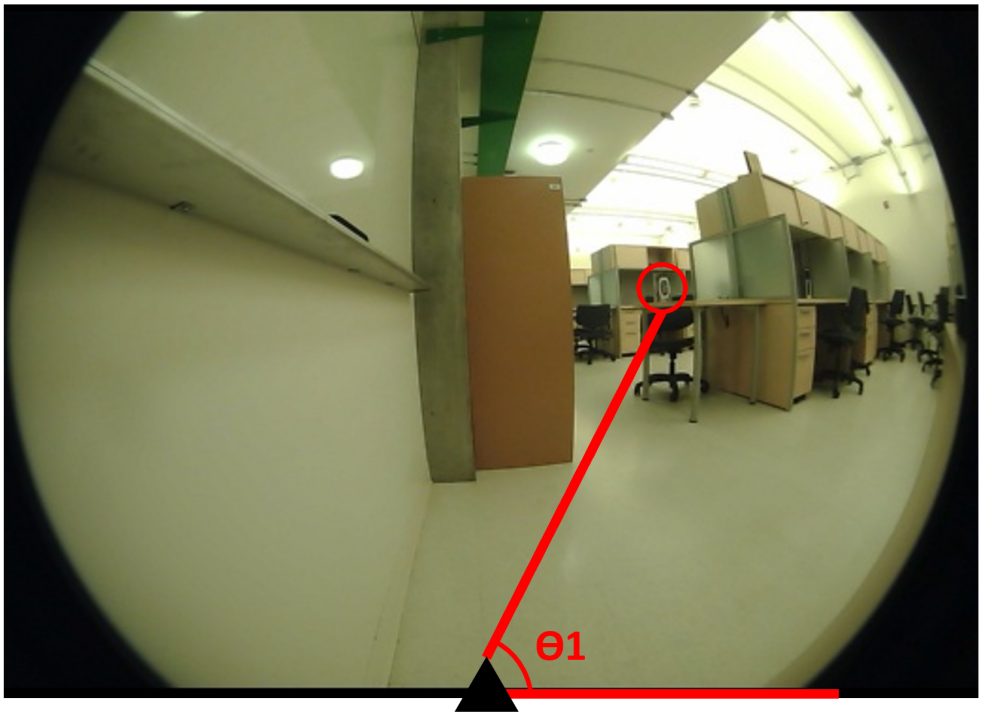

Figure 4.6: Angle $\theta 1$ labeled for DES-MFLC - Test 2

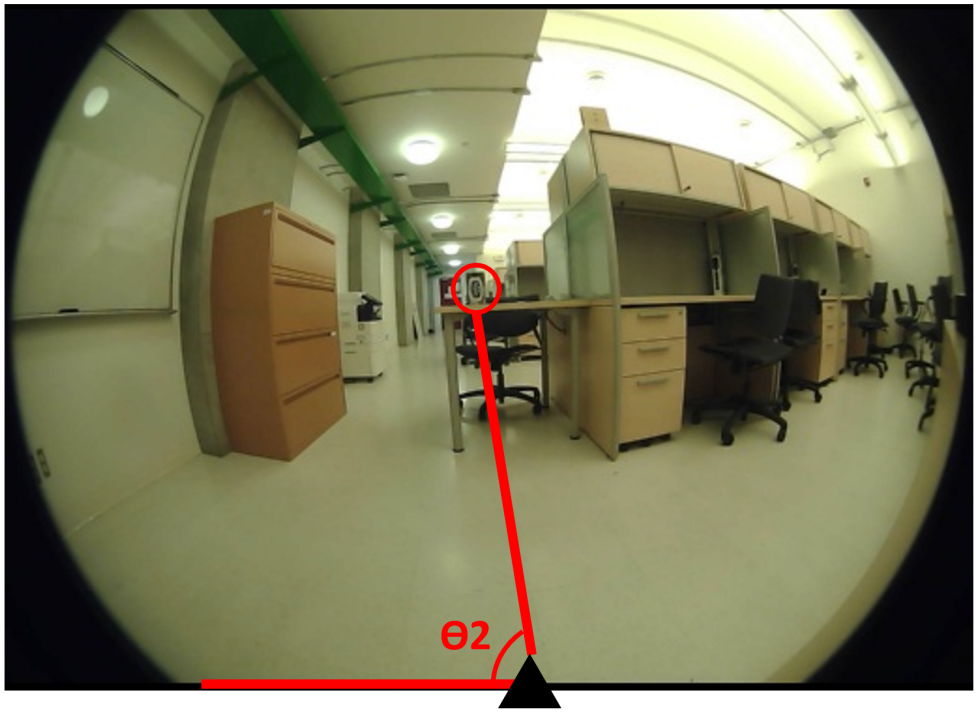

Figure 4.7: Angle $\theta 2$ labeled for DES-MFLC -Test 2

Table 4.3: Experimental results of DES-MFLC - Test 2

Figure #	**Figure 4-6**	**Figure 4-7**
Measured Distance (cm)	264.4 cm	222.3 cm
Spacing between Two Taken Pictures (cm)	139.7 cm	139.7 cm
Degree of Angles (Measured)	63°	88°
Degree of Angles (Experimental)	57.5°	86.67°
Experimental Distance (cm)		201.3 cm
Percentage Error (%)		9.44%

In Test 2, since the measured target distance was placed closer to the camera, the measurement results were more accurate than Test 1. Comparing the measured angles (63 degrees and 88 degrees) and the experimental angles (57.5 degrees in the Figure 4.6, 86.7 degrees in the Figure 4.7), the results were very similar. As a result, it provided an error of 9.44% in this test which is a more than the expected result in the system accuracy.

4.2.3 Monocular Distance Estimation - Moving test

Figure 4.8: Angle $\theta 1$ labeled for DES-MFLC - Moving test

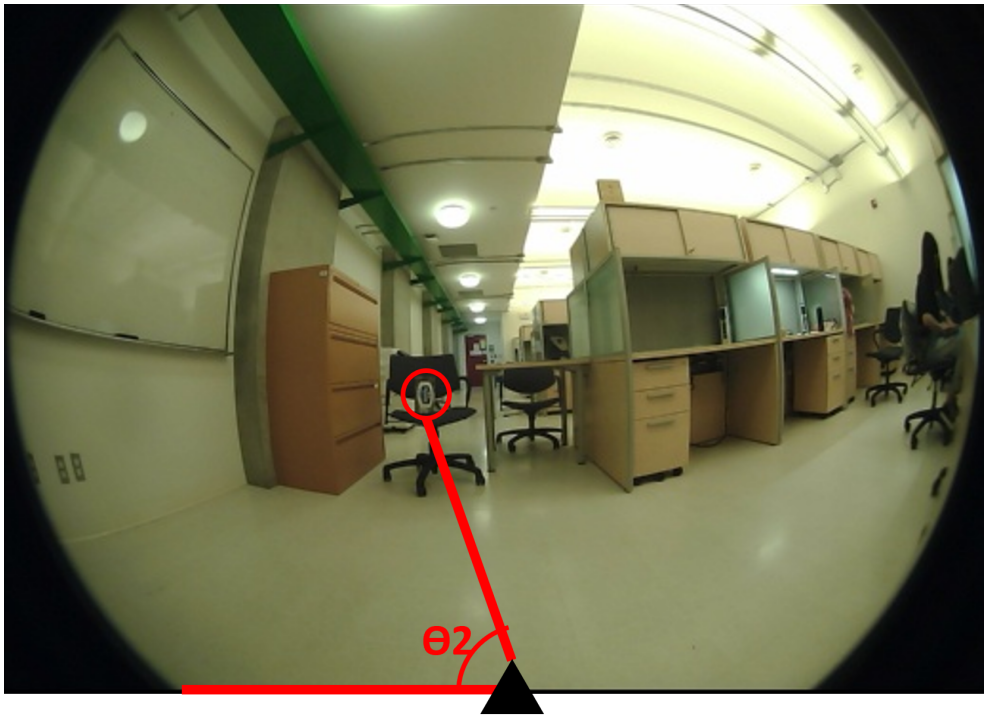

Figure 4.9: Angle $\theta 1$ labeled for DES-MFLC - Moving test

Table 4.4: Experimental results of DES-MFLC - Moving test

Figure #	**Figure 4-8**	**Figure 4-9**
Measured Distance (cm)	298.7 cm	210.1 cm
Spacing between Two Taken Pictures (cm)	127 cm	127 cm
Obstacle Moved Distance (cm)	76.2 cm	76.2 cm
Degree of Angles (Measured)	63°	80°
Degree of Angles (Experimental)	62.5°	77.5°
Experimental Distance (cm)		194.6 cm
Percentage Error (%)		7.31%

4.2.4 Binocular Fisheye Lens Cameras Spacing Test

In this case the DES-BFLC Method is used. The distance between the two cameras is an essential parameter. Since the system will be installed on a drone, there is a limit to the camera spacing for this method; therefore, this section of the experiment tested a set of pre-determined space intervals, which provided the optimal distance estimation result for

DES-BFLC. The test was executed in five spacing scenarios: 10.2 centimeters (4 inches), 15.2 centimeters (6 inches), 20.3 centimeters (8 inches), 25.4 centimeters (10 inches) and 30.5 centimeters (12 inches).

4.2.4.1 Binocular Camera Spacing Test – Test 1 (the spacing between two cameras is 10.2 cm)

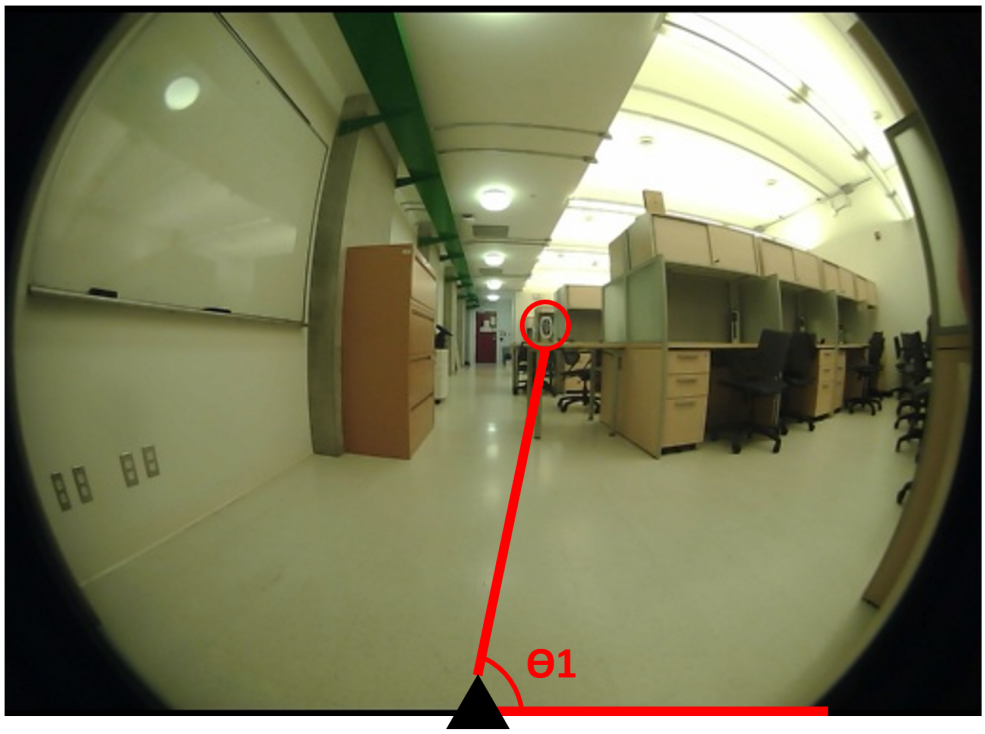

Figure 4.10: Angle $\theta 1$ for 10.2 cm spacing estimation

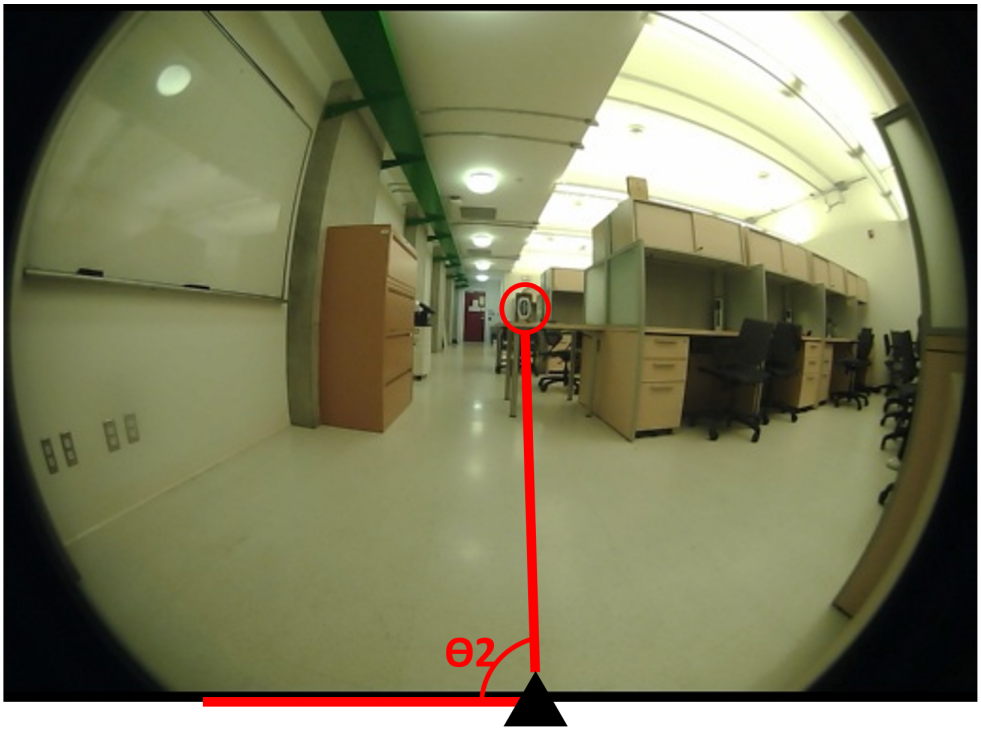

Figure 4.11: Angle $\theta 2$ for 10.2 cm spacing estimation

Table 4.5: Experimental results of DES-BFLC − 10.2 cm spacing test

Figure #	**Figure 4-10**	**Figure 4-11**
Measured Distance (cm)	258.8 cm	257.6 cm
Spacing between Two Taken Pictures (cm)	10.2 cm	10.2 cm
Degree of Angles (Measured)	83°	87°
Degree of Angles (Experimental)	85°	84.6°
Experimental Distance (cm)		141.9 cm
Percentage Error (%)	NONE	78.27%

4.2.4.2 Binocular Camera Spacing Test - Test 2 (the spacing between two cameras is 15.24 cm)

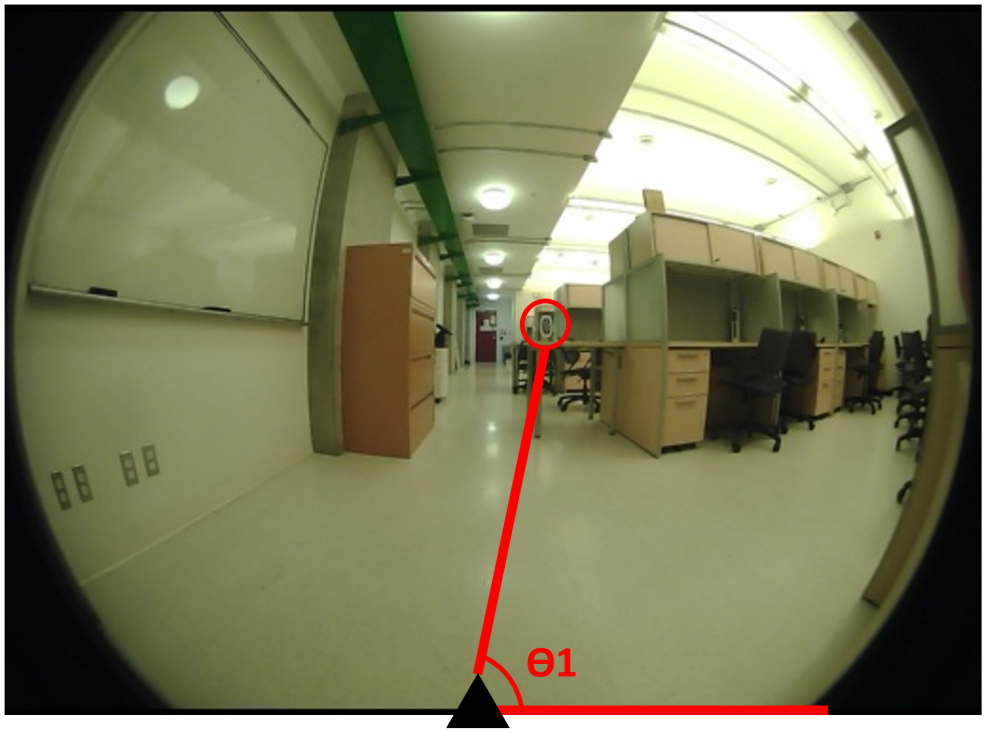

Figure 4.12: Angle $\theta 1$ for 15.2 cm spacing estimation

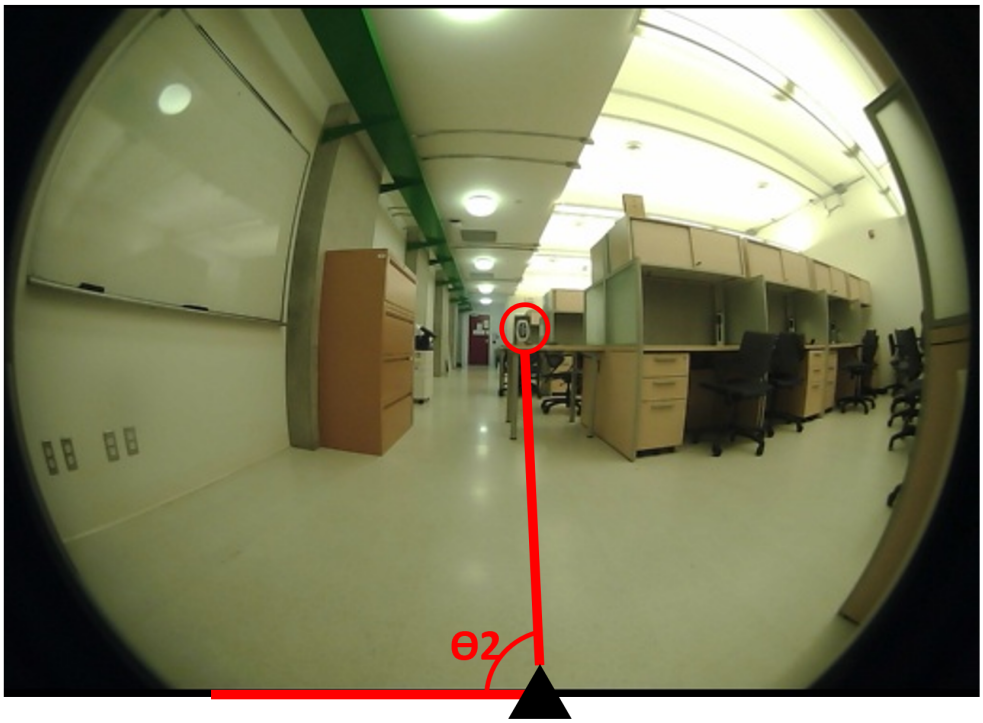

Figure 4.13: Angle $\theta 2$ for 15.2 cm spacing estimation

Table 4.6: Experimental results of DES-BFLC – 15.2 cm spacing test

Figure #	**Figure 4-12**	**Figure 4-13**
Measured Distance (cm)	258.8 cm	256.3 cm
Spacing between Two Taken Pictures (cm)	15.2 cm	15.2 cm
Degree of Angles (Measured)	83°	86.5°
Degree of Angles (Experimental)	85°	84.8°
Experimental Distance (cm)		85.7 cm
Percentage Error (%)		66.57%

4.2.4.3 Binocular Camera Spacing Test - Test 3 (the spacing between two cameras is 20.3 cm)

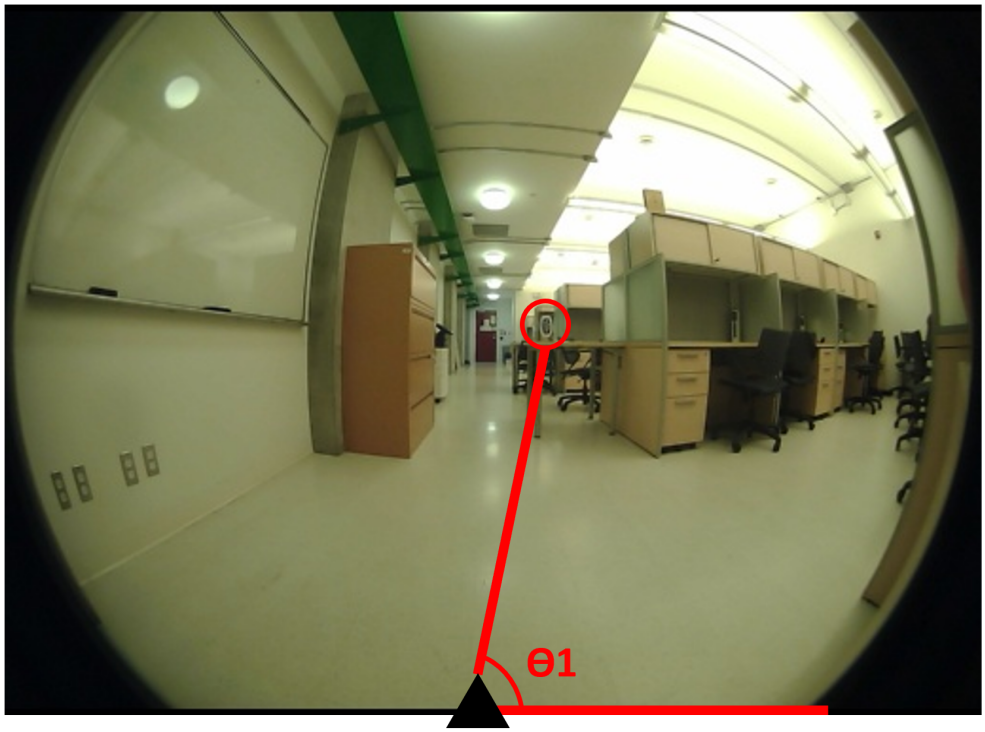

Figure 4.14: Angle $\theta 1$ for 20.3 cm spacing estimation

Figure 4.15: Angle $\theta 2$ for 20.3 cm spacing estimation

Table 4.7: Experimental results of DES-BFLC − 20.3 cm spacing test

Figure #	**Figure 4-14**	**Figure 4-15**
Measured Distance (cm)	258.8 cm	256.5 cm
Spacing between Two Taken Pictures (cm)	20.3 cm	20.3 cm
Degree of Angles (Measured)	83°	87°
Degree of Angles (Experimental)	85°	85.8°
Experimental Distance (cm)		127.1 cm
Percentage Error (%)		50.49%

4.2.4.4 Binocular Camera Spacing Test - Test 4 (the spacing between two cameras is 25.4 cm)

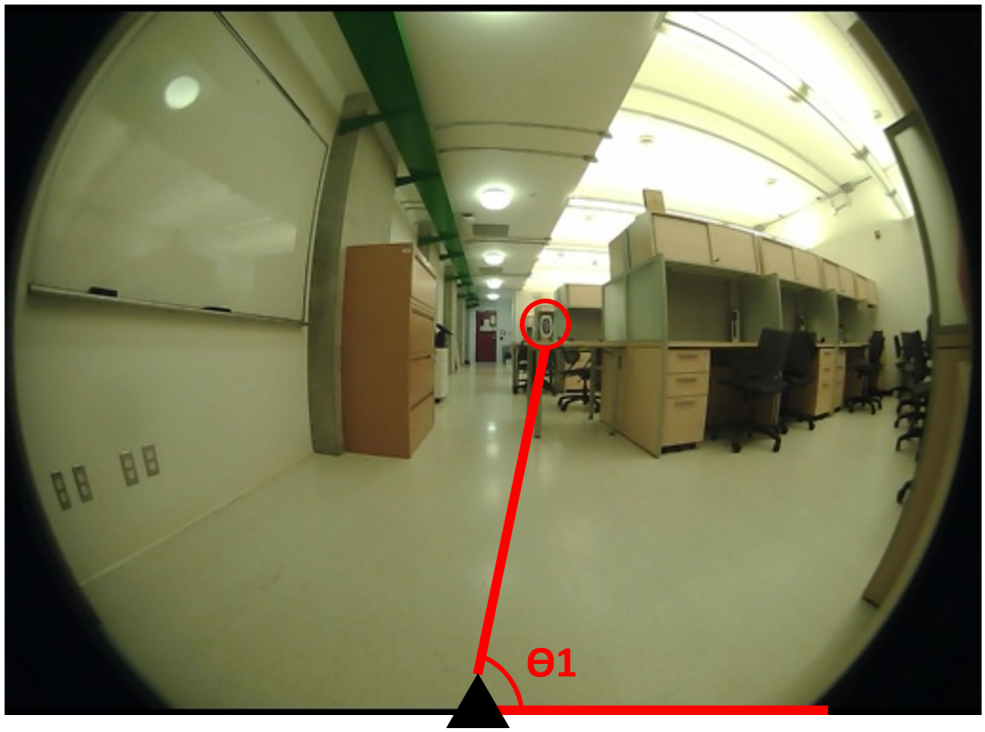

Figure 4.16: Angle $\theta 1$ for 25.4 cm spacing estimation

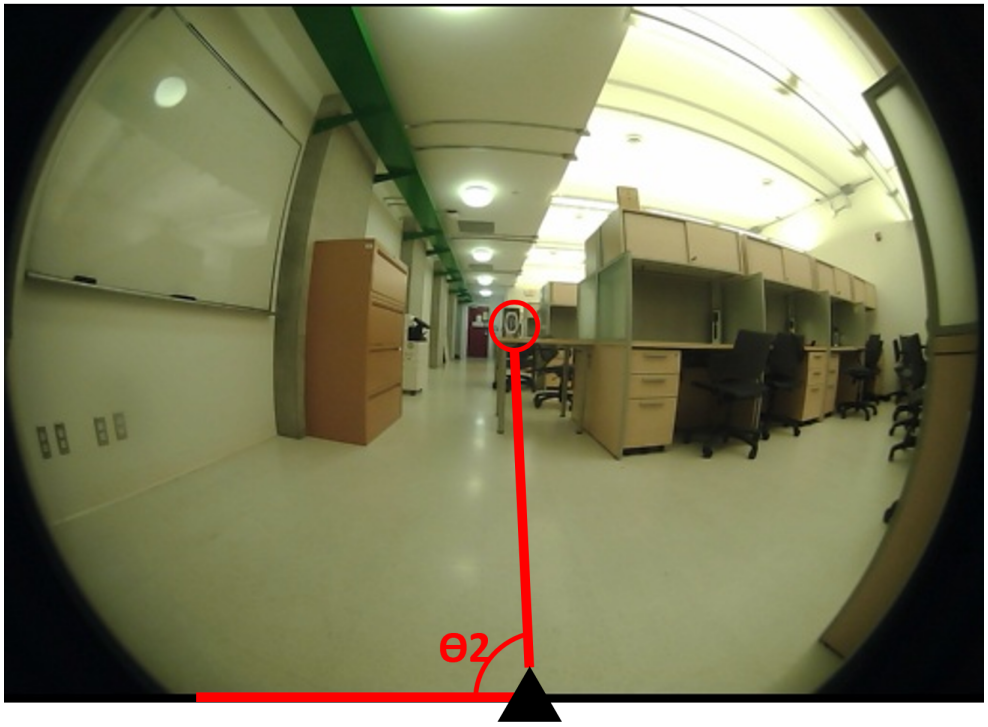

Figure 4.17: Angle $\theta 2$ for 25.4 cm spacing estimation

Table 4.8: Experimental results of DES-BFLC – 25.4 cm spacing test

Figure #	**Figure 4-16**	**Figure 4-17**
Measured Distance (cm)	258.8 cm	255.5 cm
Spacing between Two Taken Pictures (cm)	25.4 cm	25.4 cm
Degree of Angles (Measured)	83°	88°
Degree of Angles (Experimental)	85°	87.5°
Experimental Distance (cm)		193.9 cm
Percentage Error (%)		24.14%

4.2.4.5 Binocular Camera Spacing Test - Test 5 (the spacing between two cameras is 30.5 cm)

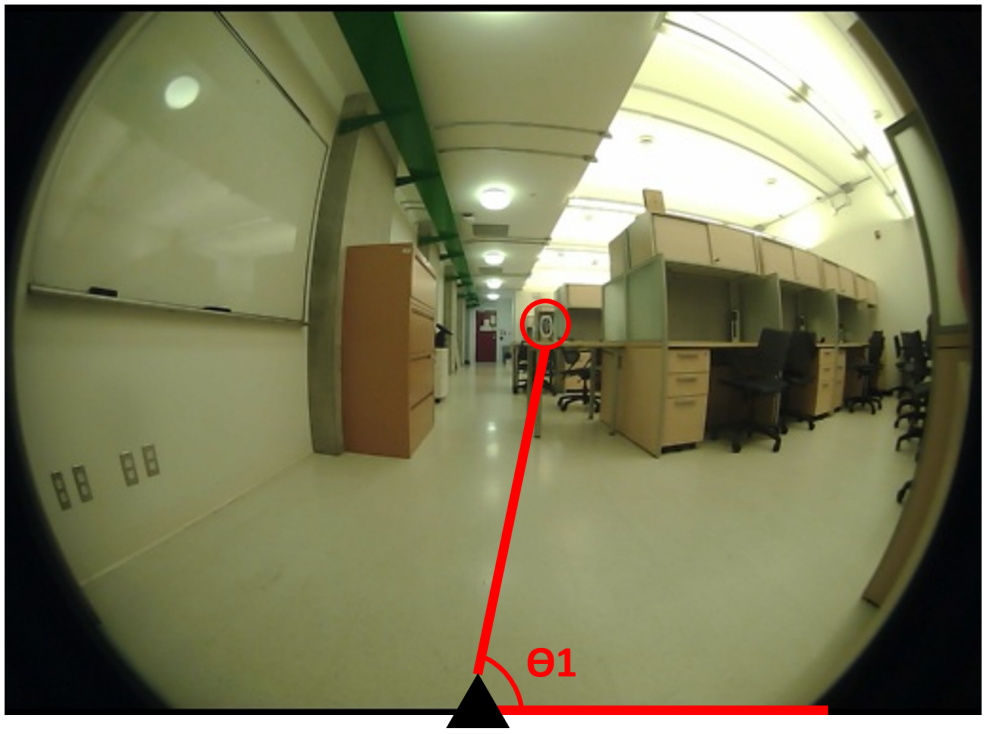

Figure 4.18: Angle $\theta 1$ for 30.5 cm spacing estimation

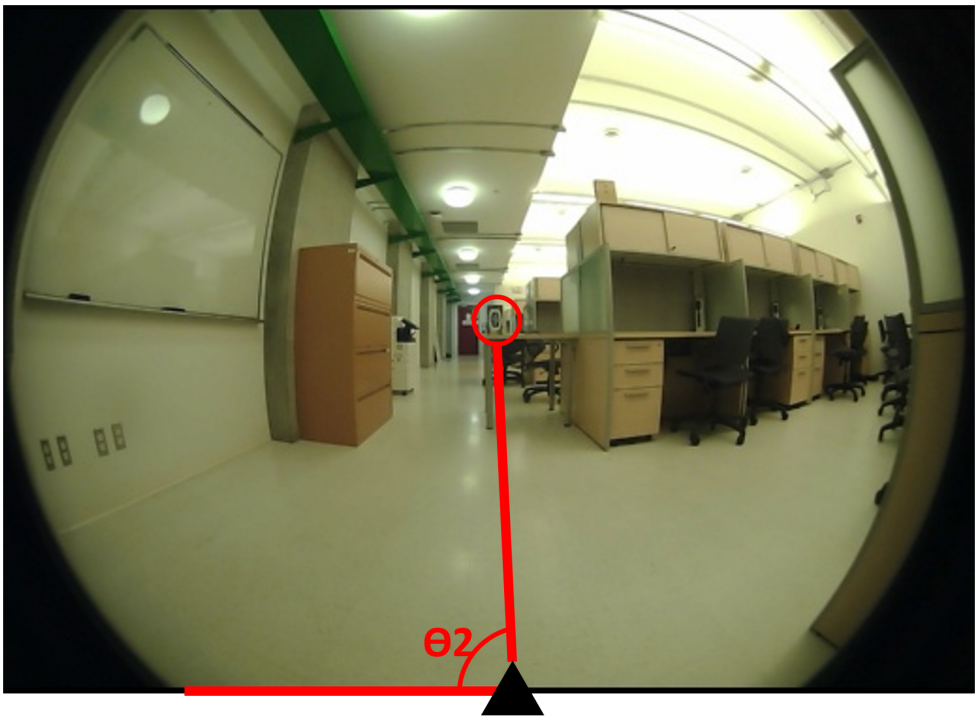

Figure 4.19: Angle $\theta 2$ for 30.5 cm spacing estimation

Table 4.9: Experimental results of DES-BFLC − 30.5 cm spacing test

Figure #	**Figure 4-18**	**Figure 4-19**
Measured Distance (cm)	258.8 cm	255.8 cm
Spacing between Two Taken Pictures (cm)	30.5 cm	30.5 cm
Degree of Angles (Measured)	83°	89°
Degree of Angles (Experimental)	85°	88.3°
Experimental Distance (cm)		260.3 cm
Percentage Error (%)		1.75%

All the experimental results were summarized and the table below is showing the details of the errors:

Table 4.10: Summary of the experimental result errors

Spacing between Two Cameras (cm)	**Degrees of Angle Error (Left) (%)**	**Degrees of Angle Error (Right) (%)**	**Distance Estimation Error (%)**
10.2 cm (4 inches)	2.41%	2.78%	78.17%
15.2 cm (6 inches)	2.41%	1.97%	66.57%
20.3 cm (8 inches)	2.41%	1.34%	50.49%
25.4 cm (10 inches)	2.41%	0.57%	24.14%
30.5 cm (12 inches)	2.41%	0.79%	1.75%

The target distance tested in this experiment is around 254 centimeters (100 inches). From Table 4.10, as the distance between the two cameras increases, the error rates of angles and the distance estimation results are continually decreasing. The decreasing error also proves the theory in Chapter 3, which asserted that the higher the distance between the cameras, the farther the measurable distance. To improve the accuracy of the drone DES-BFLC, the more distant the gap between the cameras (depends on the type of drone being used), the higher the accuracy of the results.

4.2.5 Binocular Fisheye Lens Cameras Distance Estimation Test

From the section above, it has the most accurate result when the spacing between two cameras is 30.5 centimeters (12 inches); therefore, this property will be remained for the flowing test.

4.2.5.1 Binocular Cameras Distance Estimation - Test 1

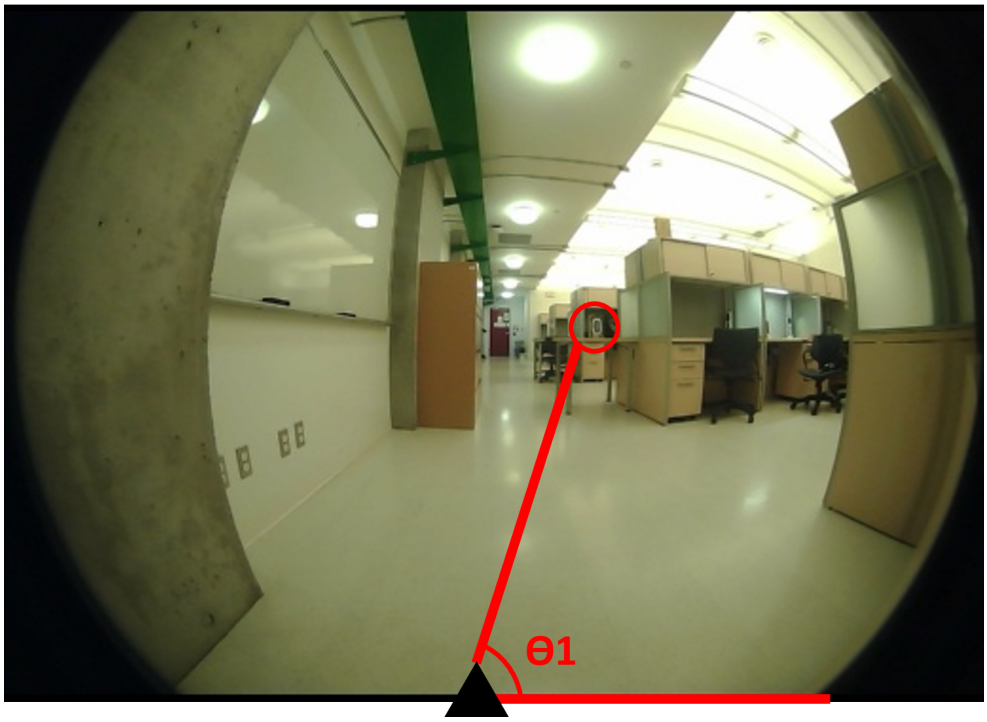

Figure 4.20: Angle $\theta 1$ labeled for DES-BFLC - Test 1

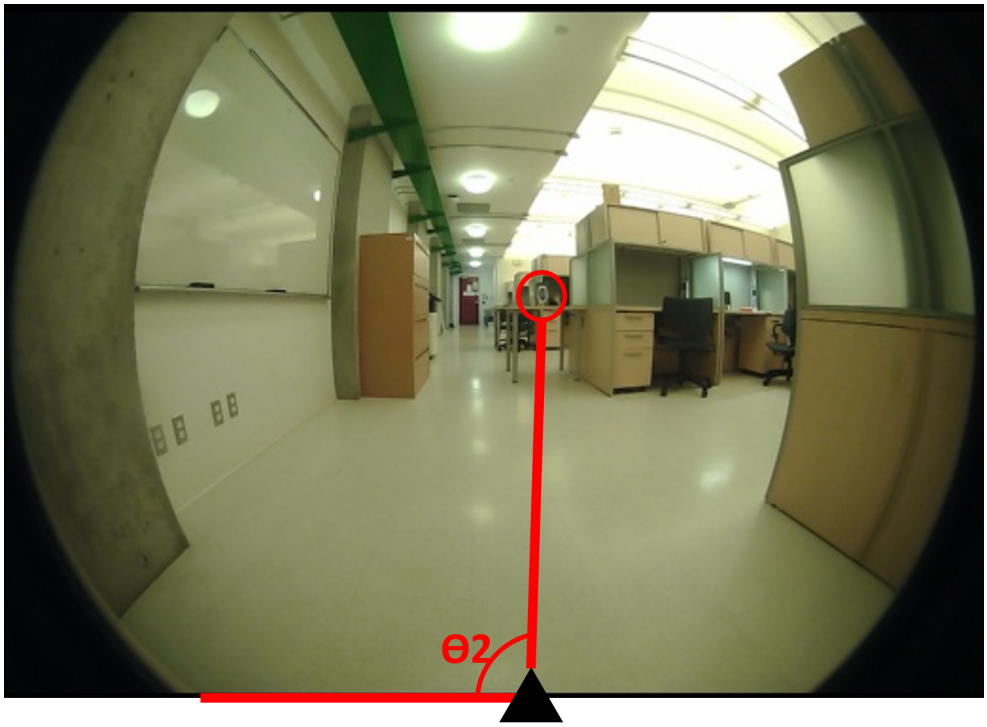

Figure 4.21: Angle $\theta 2$ labeled for DES-BFLC - Test 1

Table 4.11: Experimental results of DES-BFLC - Test 1

Figure #	**Figure 4-20**	**Figure 4-21**
Measured Distance (cm)	332.5 cm	324.1 cm
Spacing between Two Taken Pictures (cm)	30.5 cm	30.5 cm
Degree of Angles (Measured)	76°	98°
Degree of Angles (Experimental)	72.5°	100.58°
Experimental Distance (cm)		240.0 cm
Percentage Error (%)		25.61%

4.2.5.2 Binocular Cameras Distance Estimation - Test 2

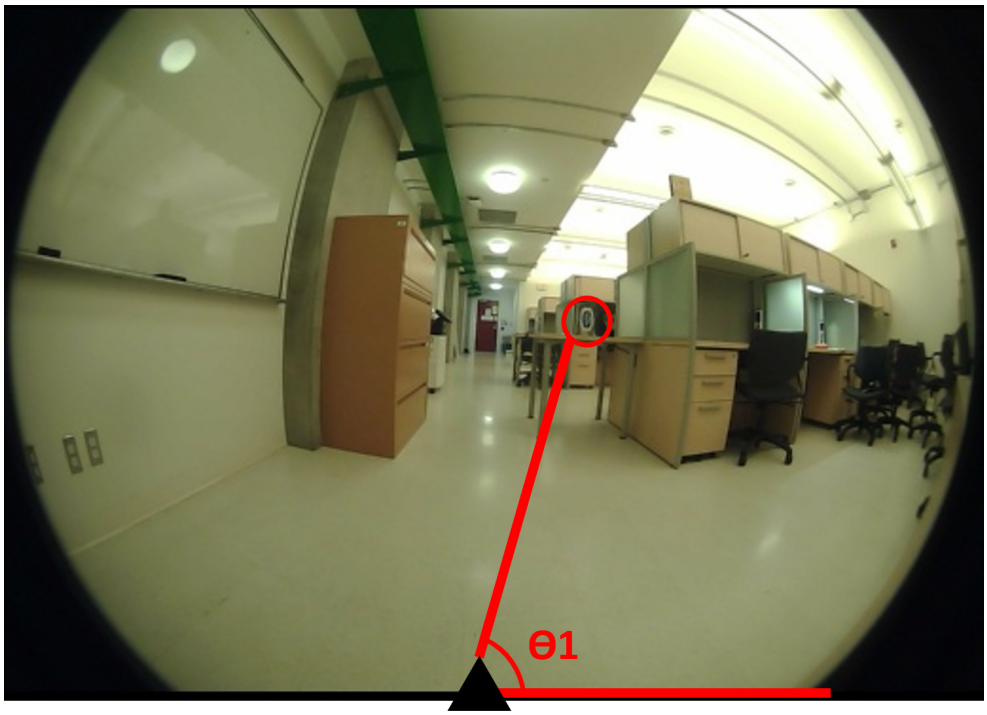

Figure 4.22: Angle $\theta 1$ labeled for DES-BFLC - Test 2

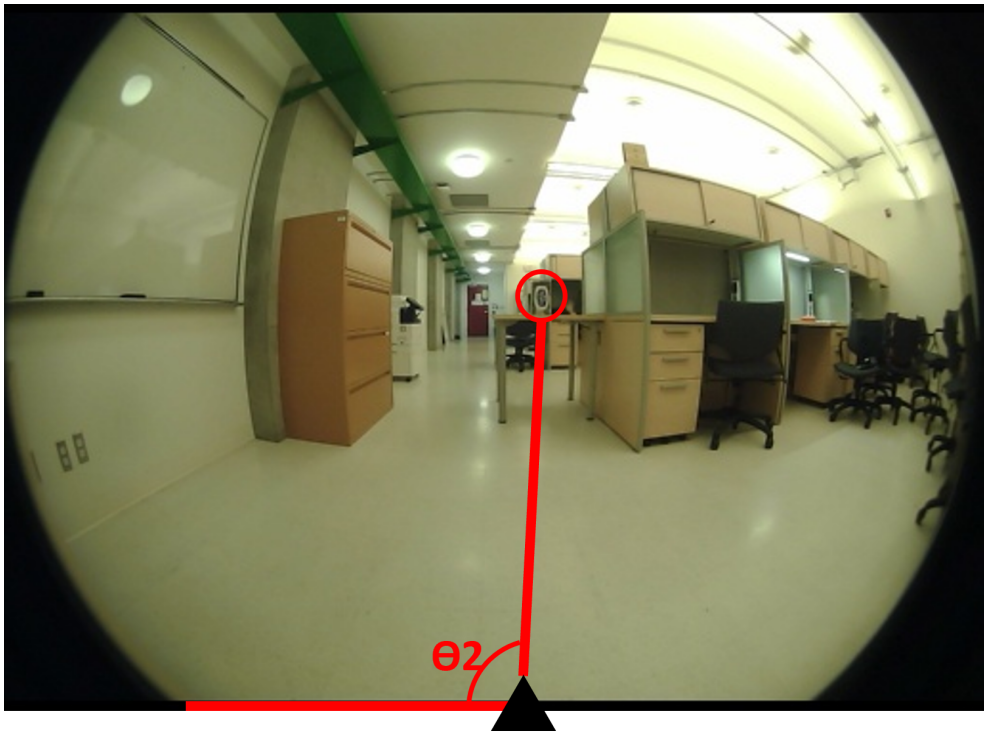

Figure 4.23: Angle $\theta 2$ labeled for DES-BFLC - Test 2

Table 4.12: Experimental results of DES-BFLC - Test 2

Figure #	**Figure 4-22**	**Figure 4-23**
Measured Distance (cm)	229.9 cm	235.2 cm
Spacing between Two Taken Pictures (cm)	30.5 cm	30.5 cm
Degree of Angles (Measured)	85°	103°
Degree of Angles (Experimental)	73.3°	98.3°
Experimental Distance (cm)		199.8 cm
Percentage Error (%)		15.03%

As seen from the two tests above, the first binocular instant ranging test measures for 324.1 cm long DE, the other one measures for 235.2 cm. It has a 25.6% and a 15.03% estimation error separately.

By using two cameras for the measurement, the system can give out an instant distance result whenever it detects the targets. With the ±20% estimation error, the binocular ranging system is accurate for instant DE.

4.2.5.3 Binocular Cameras Distance Estimation - Moving Obstacle Test

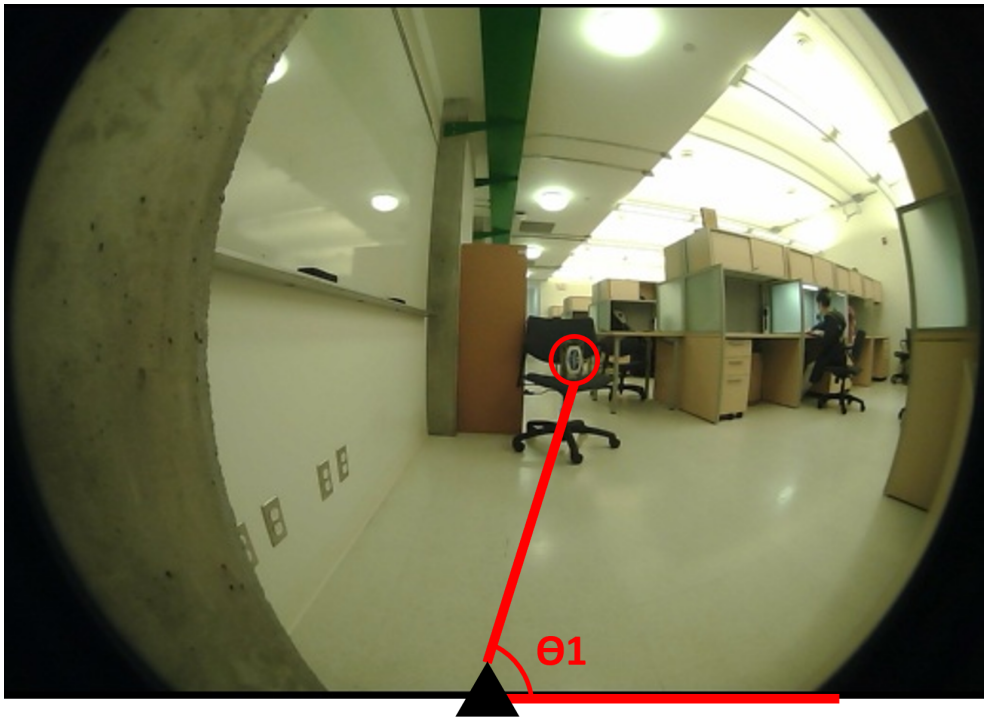

Figure 4.24: Angle $\theta 1$ labeled for DES-BFLC moving test - obstacle captured first time

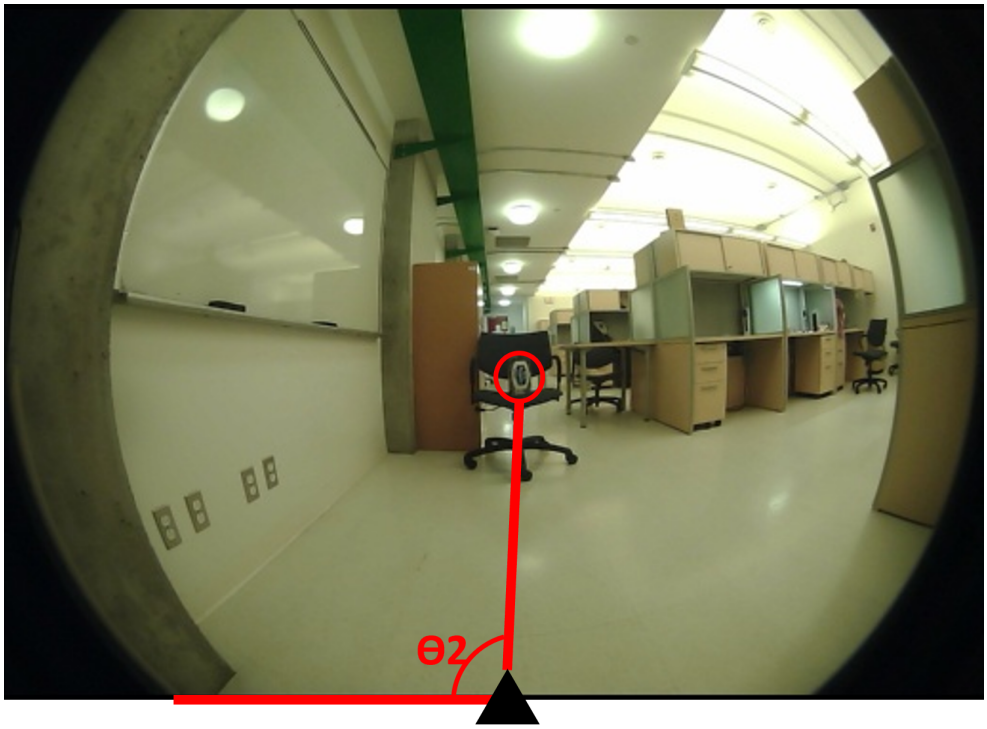

Figure 4.25: Angle $\theta 2$ labeled for DES-BFLC moving test - obstacle captured first time

Table 4.13: Experimental results of DES-BFLC moving test - first time estimation

Figure #	**Figure 4-24**	**Figure 4-25**
DES-BFLC Capturing First Time Measured Distance (cm)	199.6 cm	195.1 cm
Spacing between Two Taken Pictures (cm)	30.5 cm	30.5 cm
Degree of Angles (Measured)	102°	94°
Degree of Angles (Experimental)	79.2°	90.4°
Experimental Distance (cm)		165.6 cm
Percentage Error (%)		15.12%

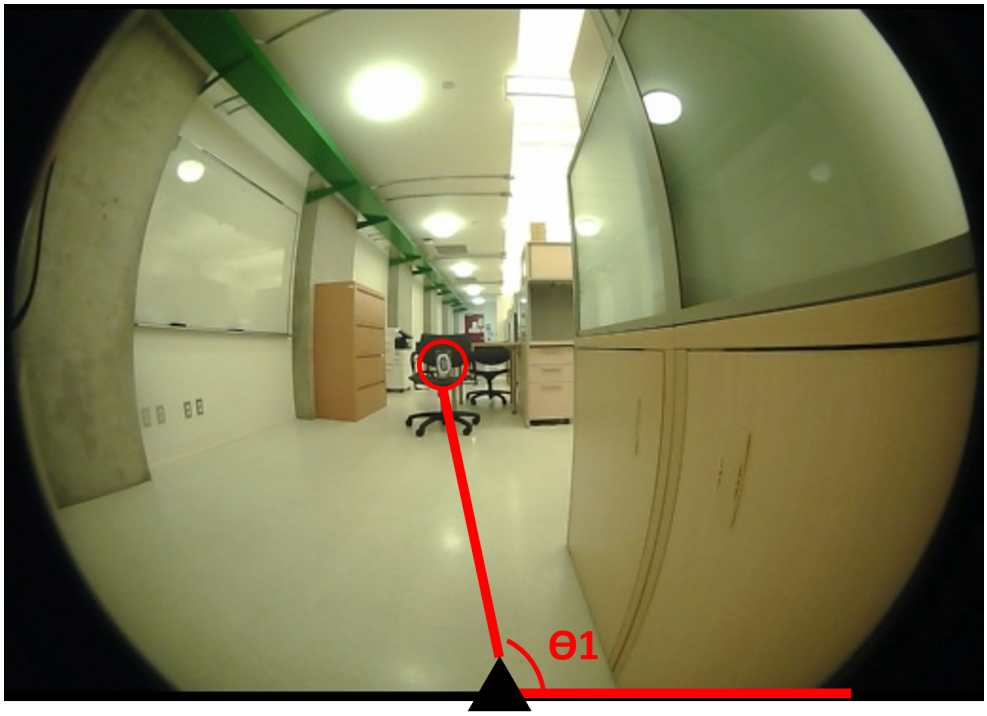

Figure 4.26: Angle $\theta 1$ labeled for DES-BFLC moving test - obstacle captured second time

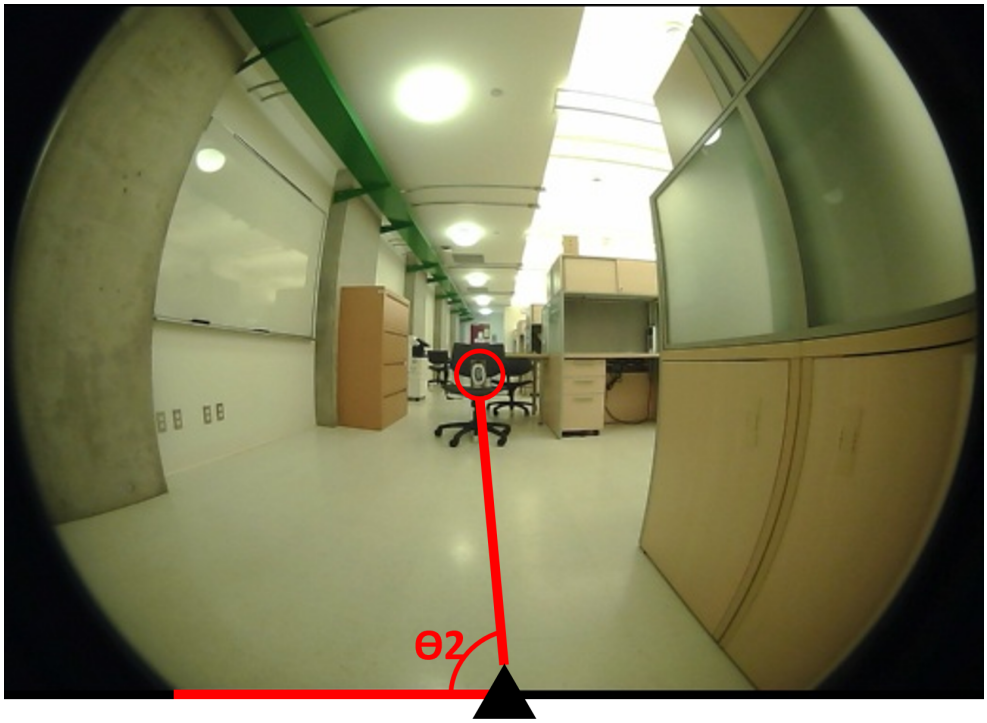

Figure 4.27: Angle $\theta 2$ labeled for DES-BFLC moving test - obstacle captured second time

Table 4.14: Experimental results of DES-MFLC moving test - second time estimation

Figure #	**Figure 4-26**	**Figure 4-27**
DES-BFLC Capturing Second Time Measured Distance (cm)	272.3 cm	274.6 cm
Spacing between Two Taken Pictures (cm)	30.5 cm	30.5 cm
Obstacle Moved Distance (cm)	63.5 cm	63.5 cm
Degree of Angles (Measured)	88°	87°
Degree of Angles (Experimental)	100°	87.5°
Experimental Distance (cm)		229.9 cm
Percentage Error (%)		16.24%

Table 4.15: Experimental results of DES-MFLC moving test - obstacle speed estimation

Distance the obstacle moved (Measured)	63.5 cm
Distance the obstacle moved (Experimental)	59.6 cm
Percentage Error (%)	6.2%
Speed of Obstacle (centimeter/second)	595.6 cm/sec

By analysing Table 4.4, Table 4.13, Table 4.14 and Table 4.15, the DES-MFLC and DES-BFLC both get accurate results. However, due to the low-cost expectation, DES-MFLC cannot have extremely accurate results as DES-BFLC has faster speed than the drone. In this condition, the DES-BFLC Method is suggested to avoid the significant error if there is enough budget. Additionally, because DES-MFLC cannot give the distance result instantly, it cannot calculate the speed of the obstacle as DES-BFLC either.

In conclusion, with excellent endurance and low procurement costs, DES-MFLC is easier to put into mass production. With the great accuracy and speed estimation, DES-BFLC will be required for diversification DES.

Chapter 5

Idealized Drone System

The main design of this drone DES is used to support the drone obstacle avoidance system in the future. The system can plan the optimal obstacle avoidance path based on the detected target distance.

The project proposed in this thesis is just a part of the final design. In addition, other parts are also essential. This section will present some ideas and recommendations for the subsequent development of this project.

5.1 Three Dimensional Full Vision Detection System for Drone

Throughout this thesis, the DES-MFLC Technique and DES-BFLC Technique are presented. By using an ultra wide angle Fisheye Lens Cameras, both of these techniques can provide horizontal and vertical 180 degrees detection.

both of these techniques can provide horizontally 180 degrees plus vertically 180 degrees detection. To further improve the detection range, two designs with 360 degrees horizontal and vertical detection are shown in Figure 5.1 and Figure 5.2. As Fisheye Lens Cameras are installed on the top and bottom of the drone, the DES can provide Three Dimensional Full Vision Detection.

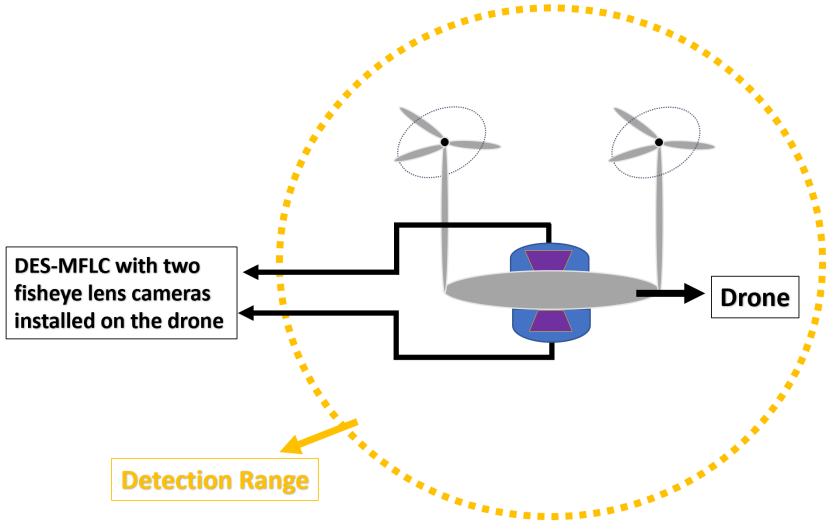

Figure 5.1: DES-MFLC three dimensional full vision detection

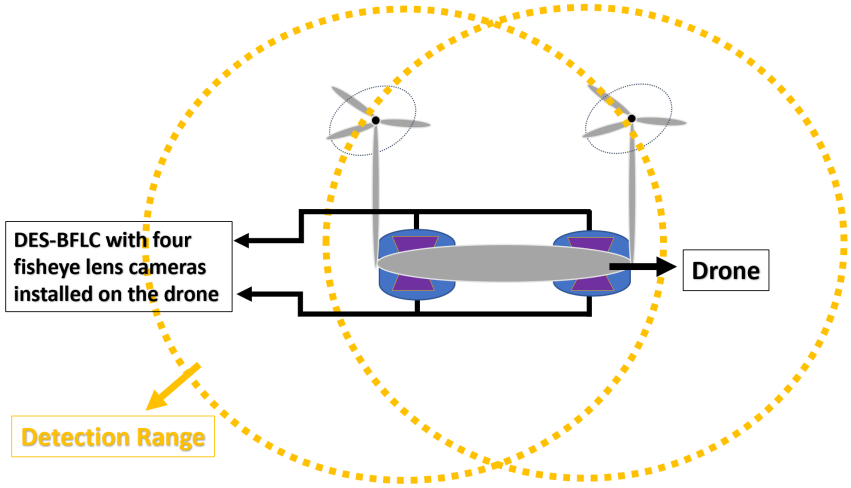

Figure 5.2: DES-BFLC three dimensional full vision detection

5.2 Navigation Lights

In order to operate the DES smoothly, it is significant to ensure that the target obstacle is detectable. This section will make assumptions and conjecture if the target is a drone.

To ensure the safety of aerospace, navigation lights are widely used on the aircraft field. Due to the high brightness of the navigation lights, it can be easily noticed day and night; therefore, this project would recommend installing a navigation light on the drone.

Navigation lights aim to increase visibility on a standard aircraft. Usually, a red and a green navigation light is located on the left and right wingtips respectively. A white light is installed on the tail of the aircraft.

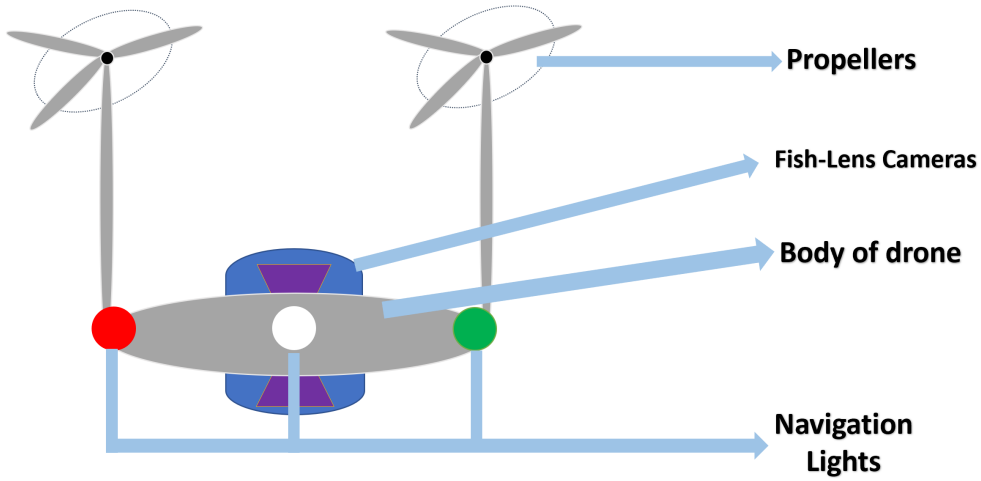

Figure 5.3: Design of drone with navigation lights

From Figure 5.3, the navigation lights that are placed on the drone are the same as the lights placed on the aircraft. As a result, if the camera captures the drone with the green navigation light on the left and red light on the right, that means the drone is flying towards the drone and vise versa. In this way, the system can clearly analyze the direction of the target drone.

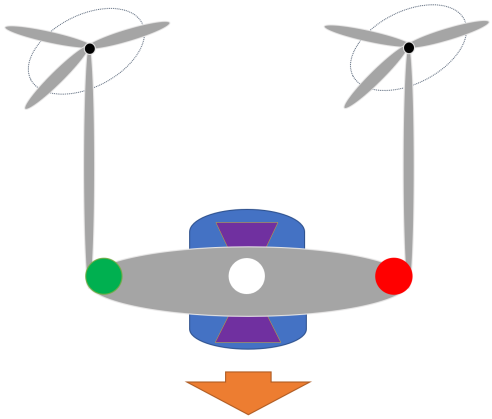

Figure 5.4: Target drone flies towards the drone

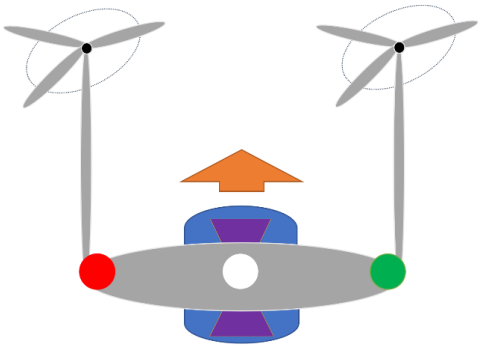

Figure 5.5: Target drone flies away from the drone

To recognize the target drones easily, a white light is placed in the middle of every drone. When the camera has captured an object with a red light on the left, green light on the right and yellow light in the middle (or a red light and green light in the opposite direction), the system can confirm the target is a drone.

Based on the high penetrating properties of navigation lights, the system can still detect the target under extreme weather.

5.3 Distance Estimation System Improvement

By using the Fisheye Lens Camera detection, the manufacturing cost will be saved while building the anti-collision system. Meanwhile, adding additional programming algorithms and hardware can improve the system performance if there is enough financial support. As stated in Chapter 3, with sufficient funds, the DES-MFLC can be replaced by DES-BFLC. Thus, it can improve the accuracy of the measurement.

In terms of algorithms, the ORB feature points detection [17] can be used for tracking the target obstacle. Feature point detection is a concept of image processing. It can extract information from the target image and determine whether it belongs to the reference image features. There are many kinds of feature points detection methods. The most common algorithms are: SIFT, SURF, ORB. ORB was brought in 2011 because it can extract and process the feature points faster than other algorithms [16]. If this algorithm is used in the system, it will improve the target tracking efficiency and its accuracy.

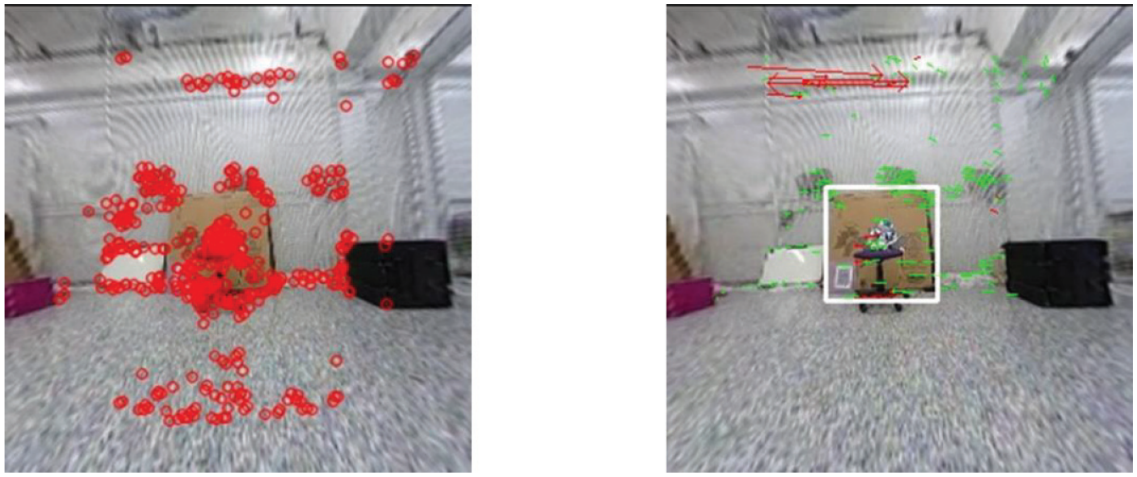

Figure 5.6: **i)** ORB feature points and **ii)** Feature point disparity between two images

Although the ORB feature points can provide favourable results, it is hard to define large obstacles if the drone is too close to them; therefore, the ultrasonic sensor can be used to improve the detection. By summarizing all the improvements, the desired design is shown below.

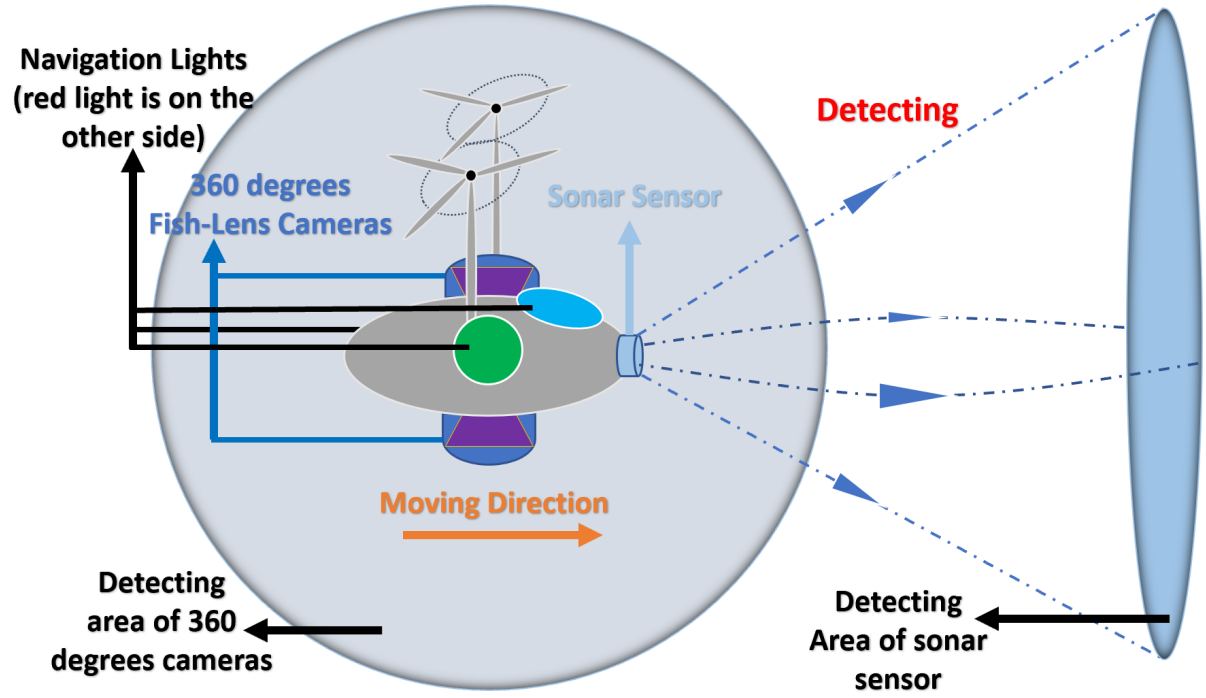

Figure 5.7: Drone Obstacle Avoidance System improved design

Chapter 6

Conclusions and Future Works

This thesis has presented an obstacle DES with a Fisheye Lens Camera, so that it can be used to achieve a low-cost vision-based OAS for a drone. By researching plenty of existing Distance Estimation Methods and OAS Techniques, the Fisheye Lens Camera Distance Estimation Method not only reduces the manufacturing costs, but also satisfies the instant feedback.

With in-depth research, the traditional vision-based Distance Estimation Method is mainly based on Stereoscopic View Techniques which requires two standard cameras. In order to improve the detection range, ultra wide angle Fisheye Lens Camera DES is presented. This DES resolves the problems of expensive prices that the lidar ranger, inaccurate distance estimation of the ultrasonic sensor and the limited detection range of standard vision-based detection.

In Chapter 4, the system was tested in DES-MFLC and DES-BFLC separately. According to the speed of the drone and the Frame per Second (FPS) of the camera used, the gap of pictures is taken is set in the range of 134.1 centimeters to 178.8 centimeters in the DES-MFLC scenario. With a long and normal distance estimation test, (long being 407.9 centimeters and normal being 222.3 centimeters) was made the DES have a 16.4% estimation error for a long-distance test and a 9.44% estimation error for a normal-distance test. As a result, the accuracy of the system is approved. In the double Fisheye Lens Camera scenario, as the spacing between the two cameras were set to be 30.5 centimeters (12 inches), a 1.75% estimation error is calculated for the 255.8 centimeters test. By analyzing the results in Table 4.10, the more distant the gap between the cameras the higher the accuracy of the results which the spacing will only be limited by the size of the testing drone.

As the moving obstacle condition for DES-MFLC and DES-BFLC is made, there were favourable results when the obstacle moved for 63.5 centimeters. Moreover, accurate obstacle speed results were also estimated in DES-BFLC test.

Some ideas and recommendations are presented in Chapter 5 for the future works of this OAS. Three Dimensional Full Vision Detection System is presented in the chapter. The system can also be improved by using the ORB feature point algorithms for obstacle detection. Additionally, ultrasonic sensors can be installed on the drone for aided detection.

In summary, the DES presented in this thesis is a promising low-cost design which can be used for Three Dimensional Full Vision OAS for the drone. This system will be completed and become more accurate in subsequent research.

Appendix A

More Experimental Results

A.1 Appendix - Test 1

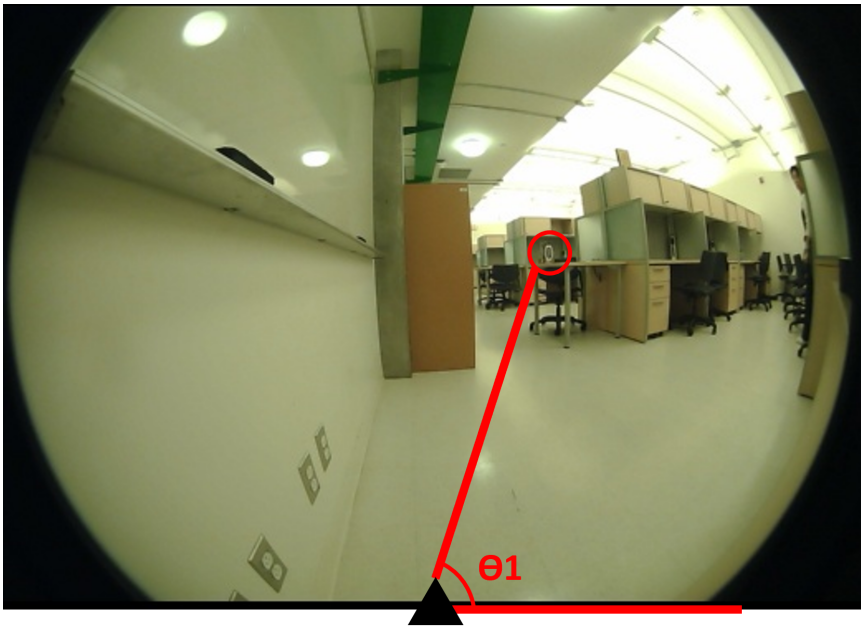

Figure A.1: Angle $\theta 1$ labeled for DES-MFLC - Appendix Test 1

Figure A.2: Angle $\theta 2$ labeled for DES-MFLC - Appendix Test 1

Table A.1: Experimental results of DES-MFLC - Appendix Test 1

Figure #	**Figure A.1**	**Figure A.2**
Measured Distance (cm)	316.5 cm	293.4 cm
Spacing between two taken pictures (cm)	152.4 cm	152.4 cm
Degree of angles (Measured)	68°	84°
Degree of angles (Experimental)	64.2°	82.5°
Experimental Distance (cm)		249.7 cm
Percentage Error (%)		14.9%

A.2 Appendix - Test 2

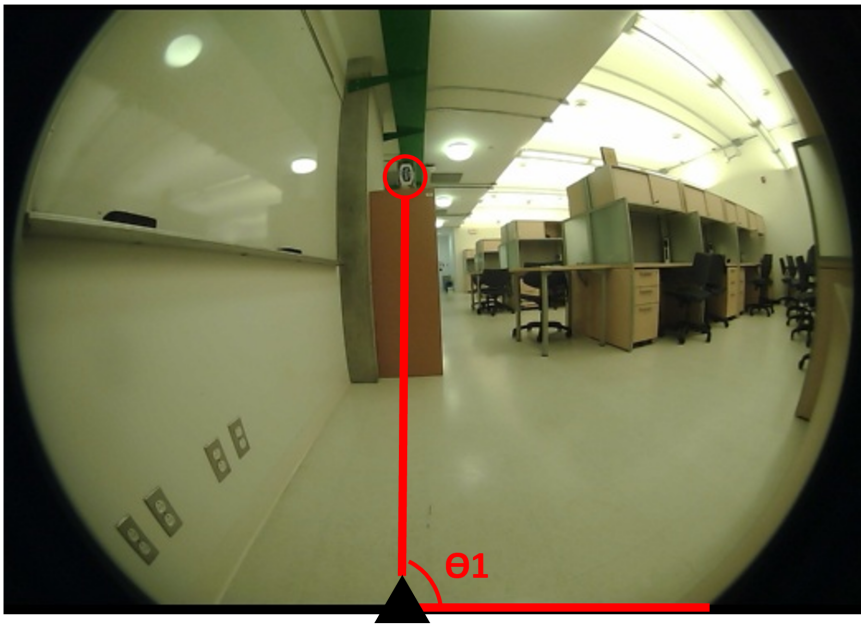

Figure A.3: Angle $\theta 1$ labeled for DES-MFLC - Appendix Test 2

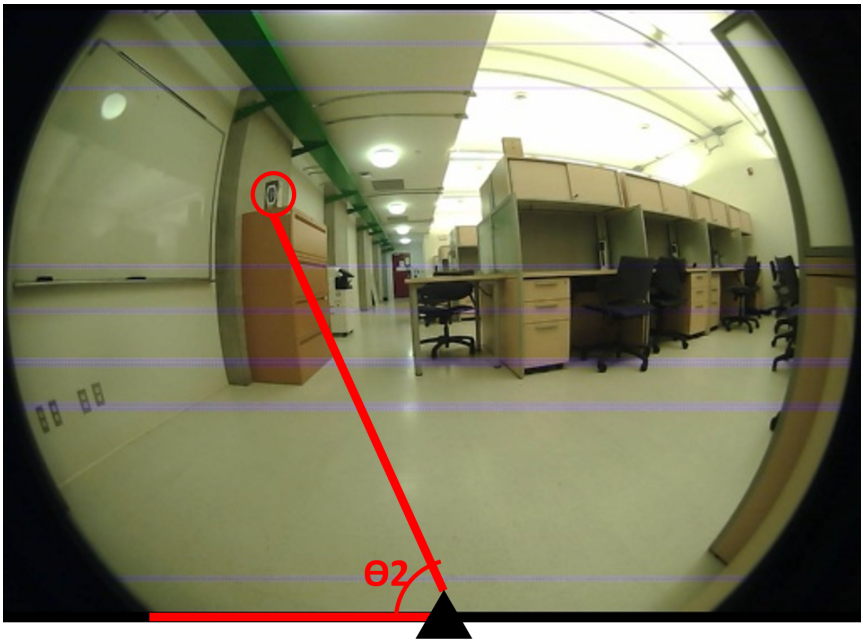

Figure A.4: Angle $\theta 2$ labeled for DES-MFLC - Appendix Test 2

Table A.2: Experimental results of DES-MFLC - Appendix Test 2

Figure #	**Figure A.3**	**Figure A.4**
Measured Distance (cm)	211.3 cm	236.5 cm
Spacing between two taken pictures (cm)	101.6 cm	101.6 cm
Degree of angles (Measured)	88°	57°
Degree of angles (Experimental)	83.3°	55.8°
Experimental Distance (cm)		154.2 cm
Percentage Error (%)		34.8%

A.3 Appendix - Test 3

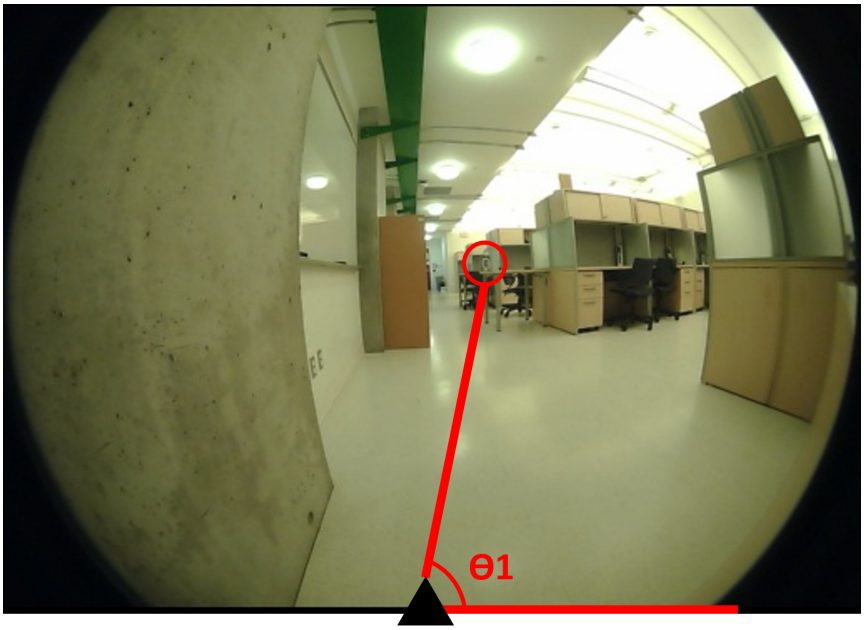

Figure A.5: Angle $\theta 1$ labeled for DES-MFLC - Appendix Test 3

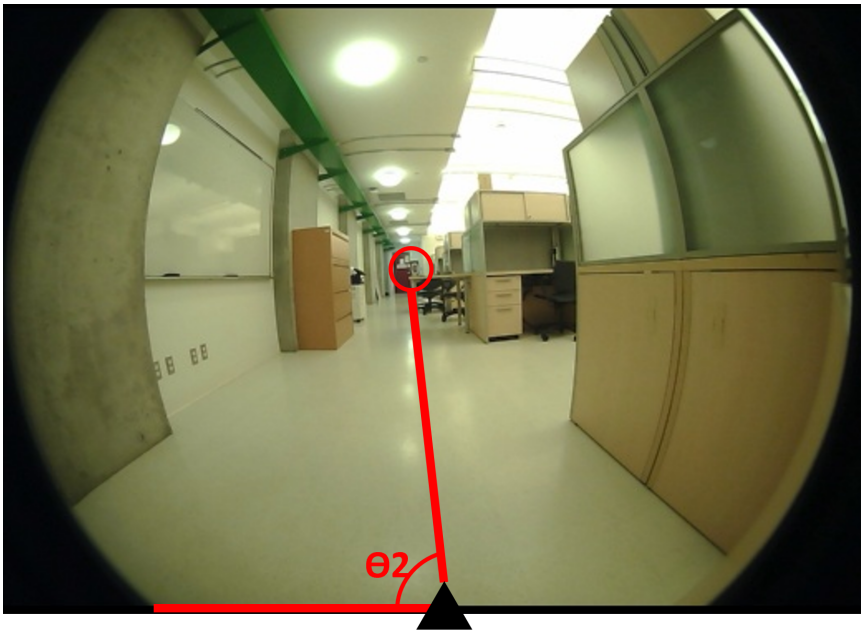

Figure A.6: Angle $\theta 2$ labeled for DES-MFLC - Appendix Test 3

Table A.3: Experimental results of DES-MFLC - Appendix Test 3

Figure #	**Figure A.5**	**Figure A.6**
Measured Distance (cm)	423.9 cm	423.926 cm
Spacing between two taken pictures (cm)	101.6 cm	101.6 cm
Degree of angles (Measured)	81°	87°
Degree of angles (Experimental)	82.9°	86.7°
Experimental Distance (cm)		557.8 cm
Percentage Error (%)		31.6%

References

[1] John F. Guilmartin. Unmanned aerial vehicle. Technical report, https://www.britannica.com/technology/unmanned-aerial-vehicle, 2019.

[2] Seoungjun Lee, Dongsoo Har, and Dongsuk Kum. Drone-assisted disaster management: Finding victims via infrared camera and lidar sensor fusion. In *2016 3rd Asia-Pacific World Congress on Computer Science and Engineering (APWC on CSE)*, pages 84–89. IEEE, 2016.

[3] Divya Joshi. Drone technology uses and applications for commercial, industrial and military drones in 2020 and the future. Technical report, https://www.businessinsider.com/drone-technology-uses-applications, 2019.

[4] John F. Guilmartin and John W.R. Taylor. Military aircraft. Technical report, https://www.britannica.com/technology/military-aircraft, 2019.

[5] Fabio Di Felice, A Mazzini, Giuseppe Di Stefano, and Giovanni Romeo. Drone high resolution infrared imaging of the lusi mud eruption. *Marine and Petroleum Geology*, 90:38–51, 2018.

[6] Allen Ferrick, Jesse Fish, Edward Venator, and Gregory S Lee. Uav obstacle avoidance using image processing techniques. In *2012 IEEE International Conference on Technologies for Practical Robot Applications (TePRA)*, pages 73–78. IEEE, 2012.

[7] Juan S Guerrero Guerrero, Aldo F Contreras González, Jose I Hernández Vega, and Leticia A Neira Tovar. Instrumentation of an array of ultrasonic sensors and data processing for unmanned aerial vehicle (uav) for teaching the application of the kalman filter. *Procedia Computer Science*, 75:375–380, 2015.

[8] Shibarchi Majumder, Rahul Shankar, and Shankar Mani Prasad. Obstacle size and proximity detection using stereo images for agile aerial robots. In *International Conference on Signal Processing and Integrated Networks SPIN*, pages 437–442. IEEE, 2015.

[9] Shishir Shah and JK Aggarwal. Depth estimation using stereo fish-eye lenses. In *Proceedings of 1st International Conference on Image Processing*, volume 2, pages 740–744. IEEE, 1994.

[10] Subaru. Fhi to introduce the new eyesight subaru's unique driving assist system with advanced safety functions. Technical report, https://www.subaru.co.jp/en/news/archives/contents, 2018.

[11] Dan Gessner. What is subaru's eyesight. Technical report, https://www.nydailynews.com/autos/street-smarts/what-is-subaru-eyesight-article-1.4042815, 2018.

[12] Shishir Shah and Jake K Aggarwal. Mobile robot navigation and scene modeling using stereo fish-eye lens system. *Machine Vision and Applications*, 10(4):159–173, 1997.

[13] Henry Horenstein. *Black and white photography.* Addison-Wesley, New York: Little, Brown, 2005.

[14] Nasim Mansurov. What is lens distortion. Technical report, https://photographylife.com/what-is-distortion, 2019.

[15] Tomoyuki Mori and Sebastian Scherer. First results in detecting and avoiding frontal obstacles from a monocular camera for micro unmanned aerial vehicles. In *IEEE International Conference on Robotics and Automation*, pages 1750–1757. IEEE, 2013.

[16] Wilbert G Aguilar, Verónica P Casaliglla, and José L Pólit. Obstacle avoidance for low-cost uavs. In *2017 IEEE 11th International Conference on Semantic Computing (ICSC)*, pages 503–508. IEEE, 2017.

[17] Arjun Kamath. *Obstacle Distance Estimation for UAV Collision Avoidance using Two-View Geometry with a Fisheye Camera.* PhD thesis, University of Kansas, 2018.

[18] Kenneth Jiang. Calibrate fisheye lens using opencv part 1. Technical report, https://medium.com/@kennethjiang/calibrate-fisheye-lens-using-opencv-333b05afa0b0, 2017.

[19] NOAA. Lidar light detection and ranging is a remote sensing method used to examine the surface of the earth. Technical report, https://oceanservice.noaa.gov/podcast/july17/nop08-historical-maps-charts.html, 2017.

[20] Hokuyo. Hokuyo utm30lx scanning laser rangefinder. Technical report, https://www.robotshop.com/en/hokuyo-utm-03lx-laser-scanning-rangefinder.html, 2019.

[21] ELECFreaks. Hcsr04 ultrasonic range finder. Technical report, https://www.robotshop.com/ca/en/hc-sr04-ultra01-ultrasonic-range-finder.html, 2019.

[22] Nils Gageik, Paul Benz, and Sergio Montenegro. Obstacle detection and collision avoidance for a uav with complementary low-cost sensors. *IEEE Access*, 3:599–609, 2015.

[23] ELP. 180degree fisheye lens. Technical report, https://www.amazon.com/180degree-Fisheye-Camera-usb-Android-Windows/dp/B00LQ854AG/ref=sr$_{13}$8?$keywords = fish + lens + cameraqid = 1565218566s = gatewaysr = 8 - 38, 2019$.